UC Davis
UC Davis Previously Published Works

Title

A borehole array data–based approach for conducting 1D site response analyses II: Accounting for modeling errors

Permalink

Authors

Pretell, Renmin
Abrahamson, Norman A
Ziotopoulou, Katerina

Publication Date

DOI

Peer reviewed

Research Paper

A borehole array data–based approach for conducting 1D site response analyses II: Accounting for modeling errors

Renmin Pretell, M.EERI[1] ⓘ**, Norman A. Abrahamson[2],**
and Katerina Ziotopoulou, M.EERI[1] ⓘ

Abstract

Site response estimates from one-dimensional (1D) site response analyses (SRAs) carry inaccuracies due to modeling and parametric errors. Modeling errors are due to the condensation of the three-dimensional (3D) wave propagation phenomenon to the vertical propagation of a horizontally polarized wave through a soil column, and parametric errors are due to the incomplete knowledge of the distributions of soil parameters, leading to the selection of nonoptimal input parameters for a site of interest. While parametric errors are traditionally handled using different soil parameters (e.g. alternative shear-wave velocity profiles), modeling errors are generally neglected. This paper proposes an approach for conducting linear elastic 1D SRAs to improve site response predictions and account for modeling errors. First, ground-motion data from borehole array sites are collected, processed, and screened for appropriateness (e.g. expected shear strains lower than 0.01%, signal-to-noise ratio higher than 3). Second, 1D SRA predictions in terms of transfer functions and amplification factors are compared against observations, and the discrepancies are quantified as residuals. Finally, the residuals are partitioned into a model bias term (c_{3D}^{SRA}), a site term ($\delta S2S_s^{SRA}$) with standard deviation ϕ_{S2S}^{SRA}, and a event- and site-specific remaining residual (δAMP_{es}^{SRA}) with standard deviation ϕ_{AMP}^{SRA}. Values for c_{3D}^{SRA} and ϕ_{S2S}^{SRA} for forward predictions are recommended. The sensitivity of the site response residuals to region, site type (1D- or 3D-like), and the applicability of findings to outcropping applications are discussed, and an example application for a hypothetical project site is presented.

[1]University of California, Davis, Davis, CA, USA
[2]University of California, Berkeley, Berkeley, CA, USA

Corresponding author:
Renmin Pretell, University of California, Davis, Davis, CA 95616, USA.
Email: rpretell@ucdavis.edu

Introduction

Predictions from one-dimensional site response analyses (1D SRAs) carry modeling and parametric errors, as well as errors intrinsic to the 1D SRA as a numerical modeling tool. The simplest approach for estimating site response consists of the propagation of the input ground motions through a soil column characterized with best-estimate shear-wave velocity (V_S) and damping profiles. Modeling errors in the predicted response come from the simplification of the 3D wave propagation phenomenon to the vertical propagation of a horizontally polarized wave through a simple 1D model, which fails to capture the effects of unmodeled non-1D site-specific features on-site response. Parametric errors are due to the lack of knowledge about the range of soil's properties and, in the case of linear elastic simulations, the most appropriate V_S and damping profiles. Finally, there are errors associated with 1D SRA as an imperfect tool when conducted with a best-estimate V_S profile and an uncalibrated amount of damping, even for sites relatively compliant with the 1D SRA assumptions. Such errors are referred to as "intrinsic errors." While parametric errors are commonly addressed by using multiple alternative input parameters, for example, baseline, upper, and lower V_S profiles (Electric Power Research Institute (EPRI), 2013), intrinsic and modeling errors are generally overlooked. This and the companion paper (Pretell et al., 2023) develop and propose an approach for conducting 1D SRAs that removes the intrinsic errors and reduce the discrepancies between observations and 1D SRA-based predictions given by the modeling errors.

The proposed approach for conducting linear elastic 1D SRAs, hereafter referred to as 1D SRAs, consists of two main parts: (1) using calibrated input parameters (damping and randomized V_S profiles) under the hypothesis that using the right amount of damping and V_S randomization removes the 1D SRA intrinsic errors, and (2) bias-correcting the response to compute the best-estimate along with the 5th' and 95th percentile median site response. Damping multipliers (D_{mul}) are used to increase laboratory-based damping values and the V_S randomization model by Toro (1995) is used to generate suites of randomized V_S profiles. Based on comparisons with borehole array data from 39 1D-like sites, it is observed that using $D_{\mathrm{mul}} = 3$ and a standard deviation for V_S randomization, $\sigma_{\ln V_S} = 0.25$, leads to more accurate median site response predictions and a reduction in the site response variability. The companion paper discusses further the calibration of damping and V_S randomization, whereas this article focuses on the quantification of the method bias and the estimation of the best-estimate median site response, and the 5th and 95th percentiles of the median site response.

A database of 495 3D-like borehole array sites from Japan and the United States is used to estimate the method bias ($c_{\mathrm{3D}}^{\mathrm{SRA}}$) and variability in the modeling error at a specific site or site term ($\delta S2S_s^{\mathrm{SRA}}$), quantified with the standard deviation $\phi_{\mathrm{S2S}}^{\mathrm{SRA}}$. Following the findings from the companion paper, 1D SRAs are conducted with $D_{\mathrm{mul}} = 3$ and $\sigma_{\ln V_S}$, and residuals are calculated for transfer functions (TFs) and amplification factors (AFs). Mixed-effects regression is used to partition the residuals into their components, and $c_{\mathrm{3D}}^{\mathrm{SRA}}$ and $\phi_{\mathrm{S2S}}^{\mathrm{SRA}}$ values for engineering applications are recommended. The protocol for conducting 1D SRAs following the proposed approach is outlined, and an example application for a hypothetical project site is presented.

Capturing modeling errors in 1D SRAs

Framework

Errors carried by 1D SRA predictions can be quantified using ground-motion data from borehole array sites. For an intensity measure (IM) of interest estimated using 1D SRAs

and the corresponding observed earthquake component "e" at a site "s," the following relation can be established:

$$IM_{es}^{obs} = IM_{es}^{SRA} + \delta_{es}^{SRA} \qquad (1)$$

where IM_{es}^{obs} and IM_{es}^{SRA} are, respectively, the observed and 1D SRA-predicted IM in natural logarithm units, and δ_{es}^{SRA} is the site response residual associated with 1D SRAs conducted using a best-estimate V_S profile and an uncalibrated amount of damping (e.g. based on laboratory testing). In this work, IM represents either TFs or AFs, estimated as the ratio of the observed or the predicted ground motion at surface and the observed (i.e. within) ground motion at depth. The residual δ_{es}^{SRA} in Equation 1 can be partitioned as:

$$\delta_{es}^{SRA} = c^{SRA} + \delta 1 D_s^{SRA} + \delta 3 D_{es}^{SRA} \qquad (2)$$

where c^{SRA} is the global 1D-SRA bias estimated from a mixed-effects regression. The site-specific term $\delta 1 D_s^{SRA}$ is due to 1D-SRA intrinsic errors (e.g. overpredictions at the site's fundamental mode) that depend on the effect of the site's damping and V_S profiles. The term $\delta 3 D_{es}^{SRA}$ is the remaining modeling residual due to non-1D features affecting the site response and the effect of variability in the ground-motion waveforms that are not accounted for by c^{SRA}. The term $\delta 3 D_{es}^{SRA}$ can be partitioned as (Al Atik et al., 2010):

$$\delta 3 D_{es}^{SRA} = \delta S2S_s^{SRA} + \delta AMP_{es}^{SRA} \qquad (3)$$

where $\delta S2S_s^{SRA}$ is the site-specific error in the analytical modeling estimated as the mean of the bias-corrected residuals at a site "s," and is referred to as "site term," and δAMP_{es}^{SRA} is the remaining unexplained bias- and site-corrected residual. The components $\delta S2S_s^{SRA}$ and δAMP_{es}^{SRA} are assumed as random variables with zero mean and standard deviations ϕ_{S2S}^{SRA} and ϕ_{AMP}^{SRA}, respectively. Replacing Equation 3 into Equation 2:

$$\delta_{es}^{SRA} = c^{SRA} + \delta 1 D_s^{SRA} + \delta S2S_s^{SRA} + \delta AMP_{es}^{SRA} \qquad (4)$$

In Equation 4, the term $\delta 1 D_s^{SRA}$ can be removed by conducting 1D SRAs with a calibrated amount of damping ($D_{mul} = 3$) and V_S randomization ($\sigma_{\ln V_S} = 0.25$). D_{mul} and $\sigma_{\ln V_S}$ are calibrated to remove the intrinsic errors, reduce the variance of site response residuals, and improve site response predictions overall. This V_S randomization should not be confused with the more common practice of randomizing V_S profiles to account for the 1D V_S variability within the footprint of a project site of interest. More generally, V_S randomization can be calibrated to capture the effect of site-specific features affecting site response for different purposes, such as to capture V_S variability or edge effects (e.g. Pretell et al., 2022). In this article, V_S randomization is used to reduce modeling errors. Given that the quantification of residuals is conducted using data from 3D-like sites, then $c^{SRA} = c_{3D}^{SRA}$. With these considerations, Equation 4 reduces to:

$$\delta_{es}^{SRA} = c_{3D}^{SRA} + \delta S2S_s^{SRA} + \delta AMP_{es}^{SRA} \qquad (5)$$

Previously, in Equations 2 to 4, δ_{es}^{SRA} is estimated from 1D SRAs conducted with a best-estimate V_S profile and uncalibrated damping values, whereas it is estimated from 1D SRAs conducted with randomized V_S profiles and calibrated damping in Equation 5. Given that borehole array data are herein used, the term δAMP_{es}^{SRA} in Equation 5 could

be further partitioned into the variability due to time histories, and due to the 3D sub-structure affecting site response:

$$\phi_{\text{AMP}}^{\text{SRA}^2} = \phi_{\text{AMP-TH}}^{\text{SRA}^2} + \phi_{\text{AMP-3D}}^{\text{SRA}^2} + 2\rho_{(\delta\text{AMP-TH}^{\text{SRA}}, \delta\text{AMP-3D}^{\text{SRA}})}\phi_{\text{AMP-TH}}^{\text{SRA}}\phi_{\text{AMP-3D}}^{\text{SRA}} \tag{6}$$

where ρ is the correlation between $\delta\text{AMP-TH}_{\text{es}}^{\text{SRA}}$ and $\delta\text{AMP-3D}_{\text{es}}^{\text{SRA}}$. For simplicity, only $\phi_{\text{AMP}}^{\text{SRA}^2}$ is estimated. All the terms in Equations 1 to 6 are frequency-dependent.

Site response predictions can be improved by accounting for $c_{\text{3D}}^{\text{SRA}}$ and $\phi_{\text{S2S}}^{\text{SRA}}$. The term $c_{\text{3D}}^{\text{SRA}}$ represents a global bias in the estimated response, and $\phi_{\text{S2S}}^{\text{SRA}}$ represents the variability in the bias-corrected 1D SRA-based median site response. The residual component $\delta\text{S2S}_{\text{s}}^{\text{SRA}}$ varies from site to site, and whether it is positive (implying underprediction) or negative (overprediction) is unknown unless borehole ground-motion data are available at a site of interest. To account for the 1D-SRA bias and the potential under- or overprediction, $c_{\text{3D}}^{\text{SRA}}$ and $\phi_{\text{S2S}}^{\text{SRA}}$ are quantified using data from a database of borehole ground motions. Note that $\phi_{\text{S2S}}^{\text{SRA}}$ is different from the within-site standard deviation in ground-motion models (GMMs), herein referred to as $\phi_{\text{S2S}}^{\text{GMM}}$, which represents the variability in amplification factors (e.g. Al Atik et al., 2010).

Proposed approach

The proposed approach for conducting 1D SRAs (1) uses D_{mul} and V_S randomization to improve site response predictions, and (2) accounts for $c_{\text{3D}}^{\text{SRA}}$ and $\phi_{\text{S2S}}^{\text{SRA}}$. The protocol for conducting 1D SRAs consists of five steps:

Step 1: site characterization. The best-estimate V_S profile is selected, and the small-strain damping after Darendeli (2001) is estimated for a site of interest. The model by Darendeli is used assuming a plasticity index (PI) of 0, a loading frequency (f_{load}) of 1 Hz, a coefficient of lateral pressure at rest (K_0) of 0.5. The same layering in the V_S profiles is considered for the development of damping profiles.

The proposed approach is developed using damping profiles estimated based on the Darendeli relation with the aforementioned values for PI, f_{load}, and K_0, and thus, they must be used in forward applications. The use of site-specific parameters could lead to an increase in damping by a factor of 2 and the underprediction of the median site response. It is expected that cases with PI, f_{load}, and K_0 that significantly deviate from the assumed values (e.g. a site on a fat clay deposit with very high PI) will require methods more advanced than the proposed approach.

Step 2: site response input parameters. A $D_{\text{mul}} = 3$ is used to increase the single small-strain damping and a suite of 50 randomized V_S profiles is generated from the best-estimate profile. The randomized V_S profiles are obtained using the Toro (1995) V_S model with $\sigma_{\ln V_S} = 0.25$ and the parameters recommended for sites with the inverse of the slowness in the top 30 m (V_{S30}) between 180 and 360 m/s. The Toro model is implemented in widely used computer codes such as STRATA (Kottke and Rathje, 2008) and DEEPSOIL (Hashash et al., 2020). The proposed approach does not require randomization of the layer thicknesses or the depth to bedrock nor the screening of V_S profile realizations. The selection of $D_{\text{mul}} = 3$ and $\sigma_{\ln V_S}$ are intended (1) to remove the commonly observed

overprediction of the site response at the fundamental mode and (2) to reduce the degree of discrepancies between observations and 1D SRA-based predictions. A detailed study on the calibration of D_{mul} and $\sigma_{\ln V_S}$ is presented in the companion paper.

Step 3: uncorrected median site response. The 50 randomized V_S profiles are used with the same single damping profile ($D_{\mathrm{mul}} = 3$) to compute the site response for each selected input ground motion. The median site response (μ_{IM}) resulting from all the 50 site responses is estimated, where IM represents Fourier amplitudes or pseudo-spectral accelerations (PSAs) at ground surface. This μ_{IM} is the uncorrected best-estimate median site response for a given input motion.

Step 4: bias correction. The estimated μ_{IM} should be bias-corrected to account for the observed overall trend to overpredict the site response around the site's fundamental mode and underpredict the high-frequency amplitudes. The bias correction is achieved by adding $c_{\mathrm{3D}}^{\mathrm{SRA}}$ to the uncorrected best-estimate median site response μ_{IM}. The resulting response is the best-estimate (bias-corrected) median site response for a given input ground motion:

Best-estimate median site response: $\mathrm{IM}_{\mathrm{BE}} = \mu_{\mathrm{IM}} + c_{\mathrm{3D}}^{\mathrm{SRA}}$

Step 5: accounting for modeling errors. The potential for site-specific modeling errors leading to a median site response that is systematically higher or lower than the average median response is accounted for. The site-specific error in analytical modeling, $\delta S2S_{\mathrm{s}}^{\mathrm{SRA}}$, can be quantified for sites where site-specific ground motion recordings are available. Given that ground motion recordings are generally unavailable, $\delta S2S_{\mathrm{s}}^{\mathrm{SRA}}$ is unknown in engineering applications. Thus, $\delta S2S_{\mathrm{s}}^{\mathrm{SRA}}$ is accounted for by considering alternative percentiles of the bias-corrected median FAS or PSA, with a 90% confidence interval:

5th percentile of the median site response: $\mathrm{IM}_{5\mathrm{th}} = (\mu_{\mathrm{IM}} + c_{\mathrm{3D}}^{\mathrm{SRA}}) - 1.65 \times \phi_{\mathrm{S2S}}^{\mathrm{SRA}}$

95th percentile of the median site response: $\mathrm{IM}_{95\mathrm{th}} = (\mu_{\mathrm{IM}} + c_{\mathrm{3D}}^{\mathrm{SRA}}) + 1.65 \times \phi_{\mathrm{S2S}}^{\mathrm{SRA}}$

All the quantities in Steps 4 and 5 are in natural logarithm units; for instance, the bias-corrected best-estimate median site response in arithmetic units is $\exp(\mathrm{IM}_{\mathrm{BE}})$.

The proposed approach is intended to be used for a site, defined as a punctual location that does not account for spatial variability of soil properties across a structure's footprint. However, the approach can be used multiple times for alternative baseline V_S profiles to account for parametric epistemic uncertainty. In the following sections, the associated components, the assumptions, and the data used in the development of the proposed approach are discussed. Finally, an example application is presented to show how the proposed approach can be used in the forward prediction of site response.

Aleatory variability and epistemic uncertainty associated with the proposed approach

A framework for the identification of sources of aleatory variability (AV) and epistemic uncertainty (EU) in ground-motion modeling (Abrahamson et al., 1990) is described in the companion paper for site response applications. The separation of AV and EU helps understand the different factors affecting the response, as well as the benefits and the limitations of a selected numerical approach. This framework is developed and discussed within the context of the proposed approach and potential extensions to it (Table 1).

The parametric AV (PAV) consists of random factors affecting the site response that can be explicitly modeled by the selected modeling approach. Such factors include randomness in time given by the ground-motion waveforms, which can be captured by using multiple time histories. These time histories lead to variability in the response for PSA at surface that can be quantified as a standard deviation associated with time histories "TH": ϕ_{AMP-TH}^{SRA}. Note that in the case of TFs or FAS, $\phi_{AMP-TH}^{SRA} = 0$.

The parametric EU (PEU) consists of the plausible alternative input parameters associated to the selected modeling approach. The PEU can include multiple suites of parameters depending on the available information and problem-specific needs (e.g. Rodriguez-Marek et al., 2020). Within the context of the proposed approach, the PEU consists of suites of input ground motions, selected based on some demand criteria, and best-estimate V_S profiles (e.g. based on different geophysical tests). The PEU also includes D_{mul} to increase damping and $\sigma_{\ln V_S}$ to randomize V_S profiles. The best-estimate and recommended values for these parameters are $D_{mul} = 3$ and $\sigma_{\ln V_S} = 0.25$, but alternative plausible values could be selected: $D_{mul} = 1-4$ and $\sigma_{\ln V_S} = 0.2 - 0.3$ (e.g. Figure 13 in the companion paper).

The modeling AV (MAV) consists of the variability in the estimated site response given the factors affecting the site response but uncaptured by 1D SRAs. These factors include the wave propagation direction and wave inclination, the presence of other wave types, the presence of a basin edge, a dipping bedrock, or complex subsurface structures. From the perspective of common 1D SRA applications, the effect of these factors on site response are regarded as random, leading to uncontrolled under- or overpredictions. Herein, the MAV is reduced by quantifying c^{SRA} and $\delta 3D_{es}^{SRA}$ in Equation 2.

Finally, the modeling EU (MEU) consists of the site-specific error in analytical modeling or site term ($\delta S2S_s^{SRA}$), its standard deviation ϕ_{S2S}^{SRA}, and the potential misestimations of c_{3D}^{SRA}, ϕ_{S2S}^{SRA}, and ϕ_{AMP}^{SRA}. The latter is quantified as standard errors (SEs). Given that c_{3D}^{SRA}, ϕ_{S2S}^{SRA}, and ϕ_{AMP}^{SRA} are herein estimated based on a large database of sites and ground-motion recordings, the SE in all cases is considered negligible (Table 1).

Relation to seismic hazard

The AV and EU components associated with the proposed approach should be consistent with seismic hazard calculations. In particular, the characterization of the seismic demand at the location of interest at depth (i.e. half-space), and the subsequent convolution of the hazard at ground surface, if required, should capture different fractions of the ground-motion variability. The seismic hazard at the half-space should be calculated using single-station sigma to remove ϕ_{S2S}^{GMM} given that site effects are explicitly modeled using site-specific 1D SRAs (Al Atik, 2015; Atkinson, 2006; Rodriguez-Marek et al., 2011, 2013). To compute the seismic hazard at the ground surface, the convolution approach proposed by Bazzurro and Cornell (2004) is recommended by EPRI (2013) and commonly used in partially non-ergodic applications in the nuclear industry (e.g. Rodriguez-Marek et al., 2014, 2021). The convolution approach requires two parameters: the median response at the ground surface (μ_{CONV}) and the standard deviation (σ_{CONV}). μ_{CONV} corresponds to the best-estimate, and the 5th and 95th percentiles of the median site response resulting from the proposed approach, whereas σ_{CONV} results from the addition of ϕ_{AMP-TH}^{SRA}. Here, we follow the approach that the component ϕ_{AMP}^{SRA} is already included in the GMM and thus is not considered in the convolution of hazard. More details are provided by Bazzurro and Cornell (2004), Pehlivan et al. (2016), and Stewart et al. (2014).

Table 1. Matrix for the separation of sources of aleatory variability and epistemic uncertainty associated with the proposed approach for conducting 1D SRAs

	Aleatory variability around the median site response	Epistemic uncertainty in the median site response
Parametric	Effect of the randomness in time on the site response, e.g., the variability resulting from using a suite of ground-motion waveforms in design: $\phi_{\text{AMP-TH}}^{\text{SRA}}$, only applicable to amplification factors.	• Alternative suites of input ground motions consistent with design criteria. • Alternative best-estimate 1D V_S profile. • Alternative values of $\sigma_{\ln V_s}$ for V_S randomization to remove $\delta 1D_s^{\text{SRA}}$: 0.2–0.3. • Alternative values of D_{mul} for increasing damping to remove $\delta 1D_s^{\text{SRA}}$: 1–4.
Modeling	Difference of the observed and analytical site response for a time history: $\delta\text{AMP-3D}_{\text{es}}^{\text{SRA}}$ Standard deviation of difference between observed and analytical site response for a time history, or the remaining unexplained residuals: $\phi_{\text{AMP-3D}}^{\text{SRA}}$.	• Error in analytical modeling: $\delta\text{S2S}_s^{\text{SRA}}$. • Standard deviation in the error in the analytical modeling: $\phi_{\text{S2S}}^{\text{SRA}}$. • Standard error of c_{3D}^{SRA}, $\text{SE}(c_{3D}^{\text{SRA}})\approx 0$ given the large database it is based on. • Standard error of $\phi_{\text{S2S}}^{\text{SRA}}$, $\text{SE}(\phi_{\text{S2S}}^{\text{SRA}})\approx 0$ given the large database it is based on. • Standard error of $\phi_{\text{AMP}}^{\text{SRA}}$, $\text{SE}(\phi_{\text{AMP}}^{\text{SRA}})\approx 0$ given the large database it is based on.

SRA: site response analyses.

Main assumptions

There are four primary assumptions associated with the proposed approach:

1. *Applicability to outcropping applications*: The calibration of D_{mul} and $\sigma_{\ln V_S}$ and the quantification of c_{3D}^{SRA} and $\phi_{\text{S2S}}^{\text{SRA}}$ are based on borehole array data. The wave canceling effects observed in borehole recordings (e.g. Bonilla et al., 2002) raise concerns as to whether findings from borehole array data are applicable to outcropping applications. An initial investigation of the validity of this assumption is presented in a later section.

2. *Perfectly measured V_S profiles*: The calibration of D_{mul} and $\sigma_{\ln V_S}$ and the quantification of c_{3D}^{SRA} and $\phi_{\text{S2S}}^{\text{SRA}}$ are based on comparisons of ground-motion observations and 1D SRA predictions, and discrepancies attributed to modeling errors. This implicitly assumes that the V_S profiles used in the 1D SRAs are flawless, which is hardly a realistic assumption (e.g. Zhu et al., 2022).

3. *Ergodicity*: c_{3D}^{SRA} and $\phi_{\text{S2S}}^{\text{SRA}}$ are estimated based on data predominantly from Japan but nevertheless considered to be applicable to any site. The ergodic assumption is required given that there are not enough borehole array sites that could potentially allow for differentiating aspects dominating site response in different regions. Removing the ergodic assumption requires (1) the collection of recorded ground motions at a site of interest, (2) the estimation of the components in Equation 5, and (3) accounting for the associated non-negligible SE of c_{3D}^{SRA} and $\phi_{\text{S2S}}^{\text{SRA}}$.

4. *Applicability to any site type*: c_{3D}^{SRA} and ϕ_{S2S}^{SRA} are recommended for any site in engineering applications. The datasets used in the estimation of c_{3D}^{SRA} and ϕ_{S2S}^{SRA} consist of 3D-like sites differentiated from 1D-like sites following a specific set of criteria that cannot be used in non-borehole array sites or in the absence of ground-motion data. Given that 93% of the sites in the database are 3D-like, it is reasonable to expect that most sites encountered in engineering practice are 3D-like. Note that the labels 1D- and 3D-like are only applicable within the context of the proposed approach and might not concur with proposed taxonomies (e.g. Pilz et al., 2022; Tao and Rathje, 2020a; Thompson et al., 2012).

Previous estimates of site response residuals

Previous studies provide estimates of c^{SRA}, ϕ_{S2S}^{SRA}, and ϕ_{AMP}^{SRA} for 1D SRAs based on different borehole datasets and damping assumptions. The following are some of these past studies (not exhaustive):

- Kaklamanos et al. (2013) conducted 1D SRAs for 100 sites from the Kiban Kyoshin Network (KiK-net) database (National Research Institute for Earth Science and Disaster Resilience (NIED), 2019) using constant damping values optimized to fit observations at each site (Thompson et al., 2012) and computed residuals for PSA. The authors found an overall underprediction as high as 0.5, except between 0.5 and 2 Hz; ϕ_{S2S}^{SRA} from 0.4 to 0.6, and ϕ_{AMP}^{SRA} of 0.3 approximately constant with frequency. Subsequent efforts (Kaklamanos and Bradley, 2018; Kaklamanos et al., 2020) identified the coarseness of V_S profiles in the KiK-net database as the factor leading to underpredictions in 1D-SRA estimates.

- Stewart and Afshari (2021) conducted 1D SRAs for 21 sites in California using three damping models and computed residuals for PSA. The authors found an overall trend of underprediction with c^{SRA} as high as 0.5 across frequencies up to 10 Hz for SRAs conducted with damping estimated based on correlations with quality factors (Q_S) and site-specific estimates of the high-frequency attenuation parameter (κ). The overall underprediction was not observed for 1D SRAs conducted with damping defined based on laboratory-based formulations (Darendeli, 2001; Menq, 2003). Stewart and Afshari estimated ϕ_{S2S}^{SRA} from 0.25 to 0.6, and ϕ_{AMP}^{SRA} from 0.2 to 0.4. The different damping formulations had a minor effect on ϕ_{S2S}^{SRA} and ϕ_{AMP}^{SRA}. The authors proposed a model for ϕ_{S2S}^{SRA} and provided recommendations for accounting for 1D SRA modeling errors.

- Zhu et al. (2022) conducted 1D SRAs for a large database of borehole and surface sites in Japan to investigate the efficacy of various methods for predicting FAS. Such methods include "full-resonance" 1D SRAs (i.e. the commonly used 1D SRAs), the square-root-impedance (SRI) 1D SRAs (Boore, 2003; Joyner et al., 1981), and the horizontal-to-vertical spectral ratio (HVSR) correction (Nakamura, 2019). Zhu et al. used two damping formulations for SRAs and found that HVSR provides more accurate predictions, whereas the SRA and SRI have an overall poor performance, attributed to high parametric and modeling errors in their dataset. The authors estimated ϕ_{S2S}^{SRA} to vary from 0.25 to 0.4 from 0.1 to 2 Hz and then rapidly increase up to 0.95 for higher frequencies. The effect of using different damping models was minor.

These studies provide valuable insights into the site response bias and variability of $\delta S2S_s^{SRA}$. In this article, a database of borehole array sites from Japan and the United States is used to estimate c_{3D}^{SRA} and ϕ_{S2S}^{SRA}, and recommended values are provided along with a framework for conducting 1D SRAs to account for modeling errors. This work is different from previous studies in that SRAs are conducted using randomized V_S profiles and residual components estimated for normalized frequencies.

Quantification of site response modeling error

Site response residuals are quantified using publicly available borehole array data from Japan and the United States (California and Alaska), downloaded from the KiK-net database, the Network for Earthquake Engineering Simulation (NEES) and the Center for Engineering Strong Motion Data (CESMD) databases.

Four cases are investigated for comparative purposes:

Case 1: Damping with $D_{mul} = 1$ and best-estimate V_S profile. Baseline case.

Case 2: Damping with $D_{mul} = 3$ and best-estimate V_S profile.

Case 3: Damping with $D_{mul} = 1$ and 50 randomized V_S profiles.

Case 4: Damping with $D_{mul} = 3$ and 50 randomized V_S profiles. Proposed approach.

Site characterization

The site characterization for 1D SRAs consists of profiles of small-strain damping, V_S, and bulk density. Given the significant impact of V_S on the predicted site response at the surface (e.g. Kaklamanos et al., 2020; Passeri et al., 2019), only sites with a measured V_S profile are used. The measured V_S profiles from Japan are provided on the KiK-net database website, whereas various sources are used for the V_S profiles of sites in the United States (Afshari et al., 2019; Gibbs et al., 2000; Holzer and Youd, 2007; Thompson et al., 2010; Thornley et al., 2019). A compromise is made to include a few sites with gaps in the V_S profile, typically at the top 1–2 m (e.g. KOCH05, SBSH01, YMTH02). Such V_S profiles are considered acceptable given that the shallow layer is expected to minimally impact the amplitudes at the site response around the fundamental mode. In these cases, V_S corresponding to the immediately underlying layer is considered for the missing portion. In cases where multiple V_S profiles are available, preference is as to profiles measured using the P-S suspension logging or any other invasive test, as they can provide high resolution regardless of the depth (e.g. Passeri, 2019). Multiple V_S are available for a minority of sites in the United States, and selecting a different profile is not expected to have an impact on this work. Figure 1 shows the location of the sites selected for the development of the proposed approach, including the 1D-like sites used for the calibration of D_{mul} and $\sigma_{\ln V_S}$ in the companion paper. The measured V_S profiles are randomized to generate 50 profiles using $\sigma_{\ln V_S} = 0.25$, calibrated to better estimate site response as discussed in the companion paper, and the V_S randomization model by Toro (1995) with the parameters recommended for sites with $V_{S30} = 180$–360 m/s. The site depths vary from 35 to 923 m, with 95% of the sites varying from 100 to 360 m, and most of them with a depth of 100 m.

The measured V_S profiles are considered flawless and discrepancies in site response predictions are attributed to modeling errors. V_S profiles could be adjusted based on the
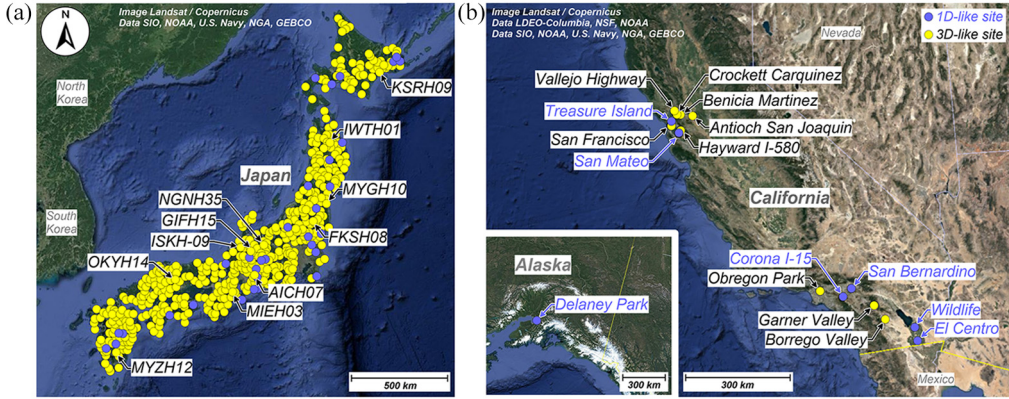
Figure 1. Borehole array site locations differentiating types as 1D- or 3D-like: (a) sites in Japan, (b) sites in California with an insert closeup view of the Delaney Park site in Alaska. *3D-like KiK-net sites used as examples throughout this paper are labeled for reference.*
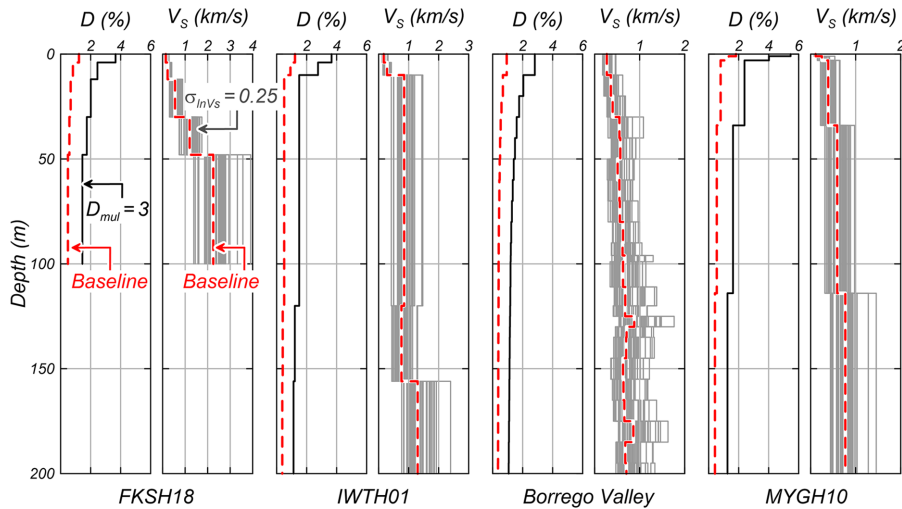

Figure 2. Examples of input V_S and damping profiles for 1D SRAs.

observed TF's fundamental mode as done by Tao and Rathje (2020a). However, this correcting approach implicitly assumes that deviations from a 1D-like TF are due to errors in the V_S profile, which might be accurate for some sites but could also be explained by non-vertical wave propagation and non-1D effects (Thompson et al., 2009). In lieu of a better approach, measured V_S profiles are used as published.

The damping profiles are estimated based on a laboratory-based relationship and density values are assumed based on V_S. The damping is estimated after Darendeli (2001) assuming PI $= 0$, $f_{load} = 1$ Hz, and $K_0 = 0.5$. The resulting damping profiles are factorized by $D_{mul} = 3$. The bulk density is assumed as 1800 kg/m³ for materials with V_S values
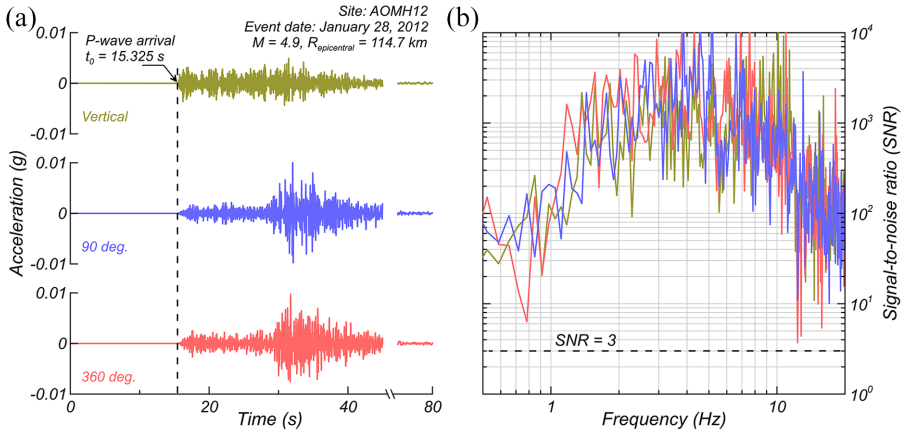
Figure 3. (a) P-wave arrival time in ground-motion recordings and (b) signal-to-noise ratio (SNR).

lower than 760 m/s, and 2200 kg/m^3 otherwise. Figure 2 shows examples of the input parameters for four sites.

Ground-motion data

Ground-motion processing. Ground-motion data are accessed from the KiK-net, NEES, and CESMD databases. In addition, the dataset for California is complemented with ground-motion recordings made available by Afshari et al. (2019). Ground motions from KiK-net and NEES are downloaded in raw format (count units) and processed using the software PRISM v2.1 (Processing and Review Interface for Strong Motion by Jones et al., 2017). Downloading the data in raw format allows for uniform processing across databases and the estimation of the event onset (t_0) using PRISM. t_0 is the time of the P-wave arrival estimated from the acceleration time history and is determined based on the rate of change of dissipated energy using the $P_{PHASE}P_{ICKER}$ algorithm (Kalkan, 2016). The t_0 differentiates the noise from the noise and earthquake signals together in the acceleration time histories (Figure 3a) and thus allows for the computation of the signal-to-noise ratio (SNR) used to assess the quality of ground-motion recordings. Data from CESMD are not available in raw format; thus, data in Volume 2 (V2) format are used, and data from Afshari et al. (2019) are used in their processed form.

Raw data are converted from counts to accelerations, baseline corrected, and filtered. An acausal filter is used with a lower corner frequency of 0.1 and a maximum of 25 Hz or higher, depending on the earthquake magnitude (Massa et al., 2010). The ground-motion data are only used up to 20 Hz as higher frequencies are affected by the instruments' anti-aliasing filters (Aoi et al., 2004). Most recordings have a sampling frequency of 200 Hz (time step of 0.005 s), and recordings with lower sampling frequencies are resampled using the frequency-domain zero-padding technique proposed by Lyons (2014) and implemented in PRISM and MATLAB (Kalkan, 2021). To estimate t_0 using PRISM for the processed data from CESMD and Afshari et al. (2019), these recordings are converted to count units using arbitrary yet reasonable shifts and scaling factors. The artificially raw recordings are then processed using PRISM, the estimated t_0 is stored for the computation of SNR using the downloaded processed recordings, and the resulting processed recordings are disregarded.

Ground-motion selection. Three criteria are considered to select ground-motion recordings appropriate for the quantification of site response residuals: (1) record component completeness, (2) SNR appropriateness, and (3) linear site response. An event is considered complete if all six components are available (three components from the sensor at depth and three from the sensor at the ground surface) or at least four horizontal components, which is the case for data from CESMD and Afshari et al. (2019). The SNR of ground-motion recordings is computed as:

$$SNR = \frac{FAS_{noise+signal}}{FAS_{noise}} \tag{7}$$

where FAS_{noise} is the Fourier amplitude spectrum of the recording from the beginning (time, $t = 0$ s) to t_0, and $FAS_{noise+signal}$ is the Fourier amplitude spectrum of the recording from t_0 to $2 \times t_0$ such that the same FAS abscissae are obtained. When available, the t_0 obtained for the vertical component is used on the two corresponding horizontal components as P waves are better observed in vertical ground motions and thus yield a more reliable t_0. Ground-motion recordings with SNR > 3 across frequencies from 0.5 Hz or at least half the site's fundamental frequency (f_0), $f/f_0 = 0.5$ up to 20 Hz are considered appropriate. In this work, the sites' f_0 is estimated as the frequency leading to the peak amplitude in the TFs computed using a within boundary condition (e.g. Kwok et al., 2007). Figure 3 shows an example of t_0 and the SNR for a set of records.

Only ground-motion recordings not expected to yield soil nonlinearities are used. Recordings potentially leading to nonlinear behavior of soils are identified using the shear-strain index (I_γ), proposed by Idriss (2011), defined as:

$$I_\gamma = \frac{PGV_{in}}{V_{S30}} \times 100\% \tag{8}$$

where PGV_{in} is the peak ground velocity of the input motions, in the same units as V_{S30}. The ground motions yielding I_γ values lower than 0.005% are expected to yield shear strains lower than 0.01% on average (Kim et al., 2016) and are thus considered appropriate for linear elastic 1D SRAs (Kaklamanos et al., 2013). The vertical recordings are not screened based on this criterion. The maximum I_γ and the minimum frequency criteria are both relaxed for sites in the United States given the limited amount of data available. For such sites, a maximum I_γ of 0.01% is considered acceptable, which is not uncommon in similar studies using ground-motion data from the United States (e.g. Stewart and Afshari, 2021; Tao and Rathje, 2020a). Also, ground motion recordings that meet the minimum SNR for frequencies up to 10–12 Hz are accepted; the impact on the amount of data at the high-frequency range is minor (Figure 4a).

Finally, all ground motions are visually screened and recordings presenting obvious anomalies are disregarded. The maximum number of events per site is set at 120 (240 recordings) to reduce computational cost. Sites with more than 120 events are re-screened to keep the recordings with the wider frequency range of acceptable SNR values. The final screened dataset consists of 534 sites, 518 from Japan and 16 from the United States (Table 2). From them, 39 sites are identified as 1D-like and used to calibrate D_{mul} and $\sigma_{\ln V_S}$ as discussed in the companion paper. The remaining 495 3D-like sites are used for the quantification of c_{3D}^{SRA} and ϕ_{S2S}^{SRA}. Figure 4 shows the number of usable recordings per frequency, and normalized frequency, and Figure 5 shows the distribution of the
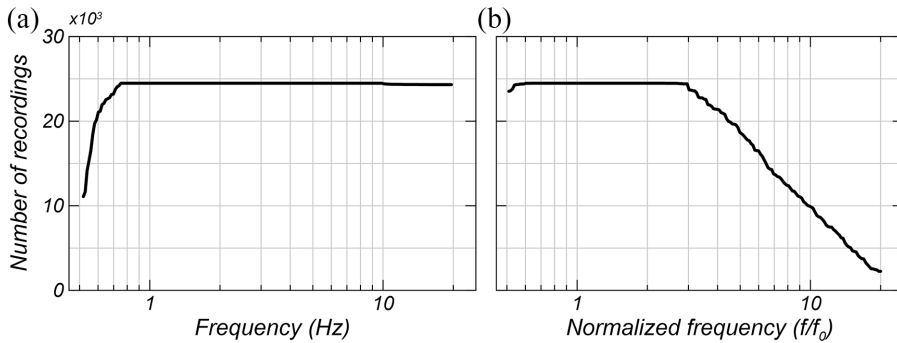
Figure 4. Number of usable ground motion recordings per frequency, f (a) and per frequency normalized by the site's fundamental frequency, f_0 (b).

Table 2. Databases and ground-motion selection criteria, including 1D- and 3D-like sites

Database	Maximum shear strain index, I_γ (%)[a]	Minimum signal-to-noise ratio, SNR	Accepted sites	Accepted events
CESMD	0.01	3[b]	12	105[c]
KiK-net	0.005	3[d,e]	518	15,541
NEES	0.01	2.5[e,f]	4	43

CESMD: Center for Engineering Strong Motion Data; NEES: Network for Earthquake Engineering Simulation; SNR: signal-to-noise ratio.
[a]Idriss (2011).
[b]SNR estimated within a frequency window from 0.5 Hz or at least half the site's frequency, up to 10 Hz. This SNR was enforced in 90% of the frequency range. Time of P-wave arrival (t_0) selected based on horizontal recordings given the absence of vertical components.
[c]Includes ground-motion recordings from the Afshari et al. (2019) database.
[d]SNR estimated within a frequency window from 0.5 Hz or at least half the site's frequency, up to 20 Hz.
[e]Vertical ground motion recordings are screened using the same SNR criteria, but no I_γ criterion is applied.
[f]SNR estimated within frequency window from 0.5 Hz or at least half the site's frequency, up to 12 Hz.

magnitude and epicentral distance of all the events in the dataset, as well as f_0 for the selected 3D-like sites. For purposes of Figure 5a, the Japanese Meteorological Agency magnitude (M_{JMA}) reported by the KiK-net recordings is considered equivalent to the moment magnitude M_w. This assumption is not unreasonable (e.g. Katsumata, 1996) and does not affect the analyses.

Site response analysis

SRAs are conducted using NRATTLE, code written by C. Mueller, modified by R. Herrmann, and included in the suite of strong-motion programs Stochastic-Method SIMulations (SMSIM) by Boore (2005). NRATTLE uses the Thomson–Haskell solution to compute the 1D SH-wave TF (Haskell, 1953; Thomson, 1950) based on a V_S profile, density, and quality factors (Q_S) or small-strain damping. The ground-motion recordings at depth are input as vertically incident SH waves into the 1D models. Each of the two horizontal components is used independently in the analysis. The borehole ground-motion recordings used as input motions capture the wavefield of incident upgoing and reflected downgoing waves. Thus, a rigid base boundary condition (e.g. Kwok et al., 2007) is
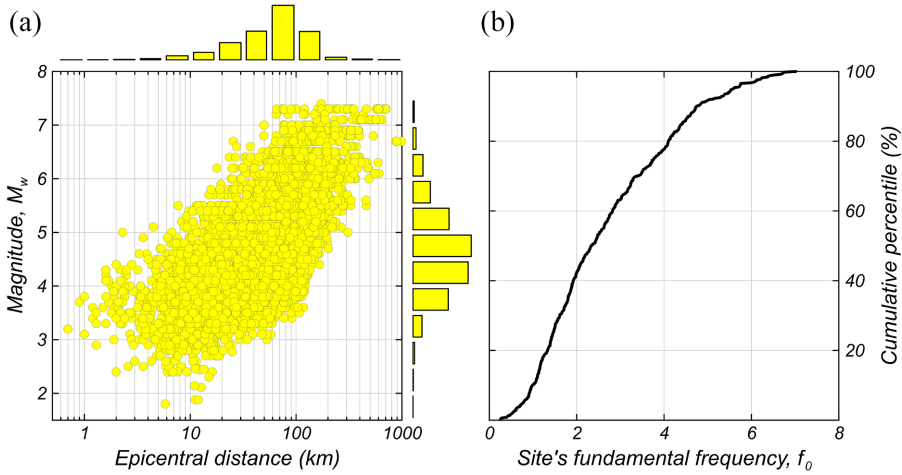
Figure 5. Data used in the development of the proposed approach: (a) distribution of epicentral distance and earthquake magnitude for selected events and (b) cumulative distribution of the site's fundamental frequencies for 3D-like sites.

assumed for the analyses. All TFs are smoothed after Konno and Ohmachi (1998) with b = 40, and PSA response spectra (5% damping) are computed using the package pyRotD (Kottke, 2018). Using other computer codes such as Shake2000 (Ordonez, 2012), STRATA (Kottke and Rathje, 2008), and DEEPSOIL (Hashash et al., 2020), leads to the same results as NRATTLE in linear elastic 1D SRAs.

Observed and theoretical TFs for four representative sites are presented in Figure 6. In general, the theoretical TFs present higher amplitudes than the observed TFs at the site's fundamental mode and often at some higher modes. The baseline theoretical TFs are more sharply peaked than the observed TFs and generally overpredict the fundamental and some higher modes. Results from the proposed approach (D_{mul} = 3 and $\sigma_{\ln V_S} = 0.25$) show smoother median theoretical TFs compared to the baseline. The smoother TFs better capture the more uniform distribution of energy across frequencies as indicated by the lower peak-to-trough ratio (e.g. Figure 6c) that is common in median observed TFs (de la Torre et al., 2021). These TFs more accurately capture the observed TFs at the fundamental mode but lead to an overall underprediction of the high-frequency amplitudes. Similar trends are observed for AFs (Figure 7).

Method bias and modeling epistemic uncertainty

The site response residuals are calculated for TFs and AFs using Equation 1 and the partition of residuals into the components $c_{\mathrm{3D}}^{\mathrm{SRA}}$, $\delta S2S_{\mathrm{s}}^{\mathrm{SRA}}$, and $\delta AMP_{\mathrm{es}}^{\mathrm{SRA}}$ is conducted using a mixed-effects regression (Pinheiro et al., 2022) to account for the correlation among the varying number of ground-motion recordings per site. Figure 8 shows $c_{\mathrm{3D}}^{\mathrm{SRA}}$ and the residuals (central 95%) for the four D_{mul}-$\sigma_{\ln V_S}$ cases. $c_{\mathrm{3D}}^{\mathrm{SRA}}$ corresponding to the baseline case (Figure 8a and b) shows a notorious overprediction of TFs and AFs at the fundamental mode (f/f_0 = 1), which is reduced as damping is increased and by using randomized V_S profiles. Between the two, D_{mul} has a weaker effect than V_S randomization in reducing the overprediction at the fundamental mode (Figure 8c and d versus 8e and f). However, the
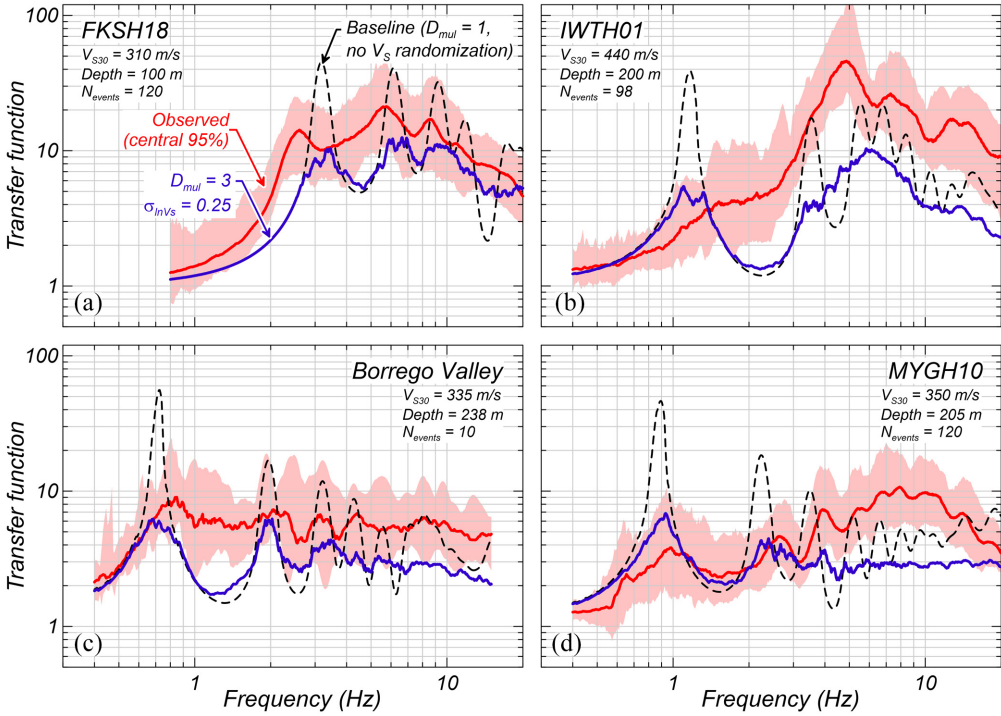
Figure 6. Comparison of observed transfer functions (TFs) and 1D SRA-based TFs for Case 1: Baseline (damping with $D_{mul} = 1$ and best-estimate V_S profile), and Case 4: Proposed approach (damping with $D_{mul} = 3$ and randomized V_S profiles). Results for four example borehole array sites: (a) FKSH18, (b) IWTH01, (c) Borrego Valley, and (d) MYGH10.
The median TFs in Case 4 result from TFs corresponding to 50 randomized V_S profiles.

proposed D_{mul}-$\sigma_{\ln V_S}$ combination leads to a nearly unbiased prediction of TFs and AFs, with c_{3D}^{SRA} from -0.5 to 0.5 (Figure 8f versus 8 h). The underprediction of TFs is addressed in Step 3 of the proposed approach.

The estimated ϕ_{S2S}^{SRA} and ϕ_{AMP}^{SRA} are presented in Figure 9. ϕ_{S2S}^{SRA} is around 0.6 for TFs and from 0.4 to 0.5 for AFs, and ϕ_{AMP}^{SRA} is nearly constant around 0.4 and 0.3 for TFs and AFs, respectively. These results indicate that a significant reduction of ϕ_{S2S}^{SRA} of TFs is obtained by the proposed D_{mul}-$\sigma_{\ln V_S}$ in the f/f_0 range from 1.6 to 8, and relatively minor differences are observed at lower and higher f/f_0 (Figure 9a). ϕ_{S2S}^{SRA} of AFs presents a relatively modest reduction of 0.15 from Case 1 to Case 4 across frequencies (Figure 9b). ϕ_{AMP}^{SRA} of TFs is the same for all the D_{mul}-$\sigma_{\ln V_S}$ scenarios given that TFs scale proportionally with D_{mul} and $\sigma_{\ln V_S}$ at a given frequency (Figure 9c). Finally, ϕ_{AMP}^{SRA} of AFs presents a reduction of about 0.2 at the fundamental mode for the proposed D_{mul}-$\sigma_{\ln V_S}$ and around 0.1 at higher frequencies (Figure 9d).

Conducting 1D SRAs following the proposed approach leads to an overall reduction in c_{3D}^{SRA} and ϕ_{S2S}^{SRA}. A reduction in c_{3D}^{SRA} indicates that the estimated FAS or PSA at the surface is more accurate and only a small bias correction is required. A smaller ϕ_{S2S}^{SRA} indicates more confidence in the estimated response. Recommended models for c_{3D}^{SRA} and ϕ_{S2S}^{SRA} are provided for various f/f_0 or normalized period (T/T_0) in Table 3, and presented in Figures 8g and h, and 9a and b. The estimated response at surface is valid for frequencies
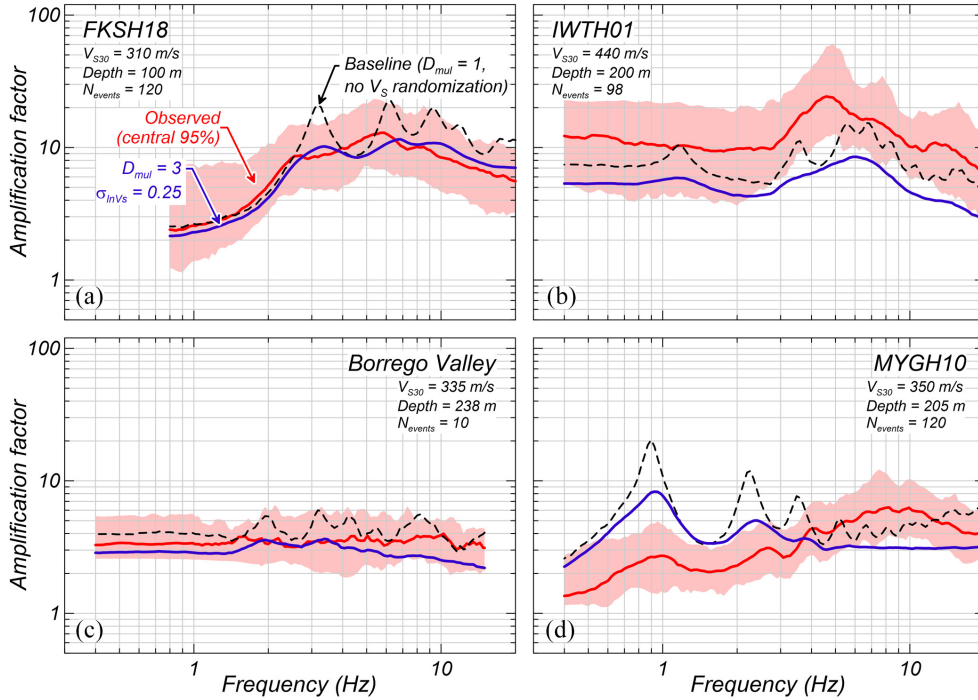
Figure 7. Comparison of observed amplification factors (AFs) and 1D SRA-based AFs for Case 1: Baseline (damping with $D_{mul} = 1$ and best-estimate V_S profile), and Case 4: Proposed approach (damping with $D_{mul} = 3$ and randomized V_S profiles). Results for four example borehole array sites: (a) FKSH18, (b) IWTH01, (c) Borrego Valley, and (d) MYGH10. *The median AFs in Case 4 result from all the median AFs estimated from each ground motion recording propagated through 50 randomized V_S profiles (i.e. median of median AFs).*

captured by the 1D model, approximately higher than the site's f_0. In this work, the quantities c_{3D}^{SRA} and ϕ_{S2S}^{SRA} are estimated using ground-motion data from 0.5 to 20 Hz, normalized frequencies f/f_0 from 0.5 to 20 (Figure 4), recorded at borehole array sites within TF-based f_0 from 0.25 to 7 Hz (Figure 5b). The site response at frequencies outside these bounds can be estimated using GMMs.

These results are consistent with findings from previous studies that have used a similar database. The results are not fully comparable as such studies did not use the normalized frequency in the estimation of the residual analysis, but some trends can be observed. For TFs, the estimated ϕ_{S2S}^{SRA} is higher at low frequencies and lower at high frequencies compared to Zhu et al. (2022), and a similarly minor effect of damping models is observed. For AFs, the estimated c_{3D}^{SRA} is lower (i.e. closer to zero or more negative) than Kaklamanos et al. (2013), although with similarly low values across frequencies. ϕ_{S2S}^{SRA} of AFs is slightly lower than the estimated by Kaklamanos et al. (2013), and ϕ_{AMP}^{SRA} of AFs similar. Various studies showed very consistent trends in the ϕ_{AMP}^{SRA} estimates.

Comparison against borehole array data

To illustrate the predictive capability of the proposed approach, TFs and AFs are computed for five KiK-net sites and results compared to observations. These sites $\delta S2S_s^{SRA}$ in
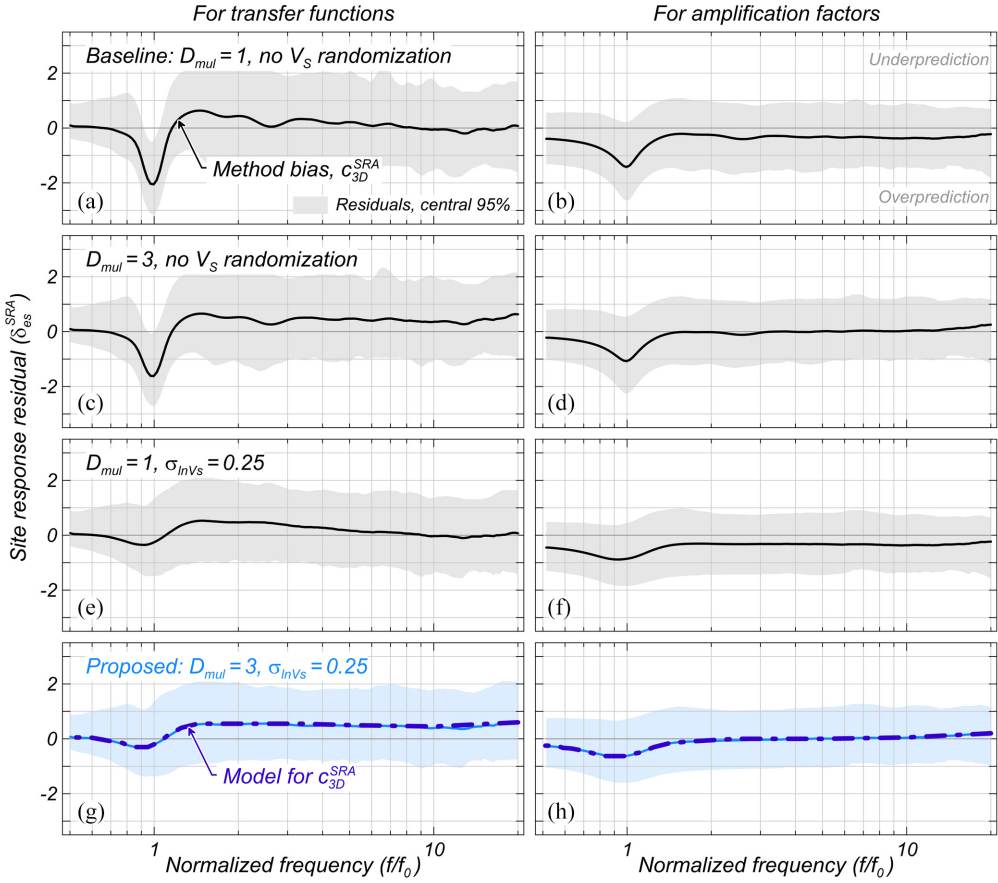
Figure 8. Comparison of site response method bias (c_{3D}^{SRA}) and residuals (central 95%) in transfer functions and amplification factors. (a) and (b): Case 1, baseline (damping with $D_{mul} = 1$ and best-estimate V_S profile); (c) and (d): Case 2 ($D_{mul} = 3$ and best-estimate V_S profile); (e) and (f): Case 3 ($D_{mul} = 1$ and randomized V_S profiles with $\sigma_{\ln V_S} = 0.25$); and (g) and (h): Case 4, proposed ($D_{mul} = 3$ and $\sigma_{\ln V_S} = 0.25$).

AFs at $f/f_0 = 1$ spanned across from underprediction to overprediction, as shown in Figure 10. The cumulative distributions of $\delta S2S_s^{SRA}$ estimated based the recommended c_{3D}^{SRA} models (Table 3) including the approximate location of the five selected KiK-net sites are presented in Figure 10a and b for TFs and AFs, respectively. Note that the ranking of a site's $\delta S2S_s^{SRA}$ in AFs does not uniformly translate to the ranking in TFs. This is particularly evident for the site SZOH37.

Figure 11 illustrates a comparison between observations and results from the proposed approach for the five KiK-net sites in terms of TFs and AFs. The best-estimate responses show an overall ability to capture well the median observed responses (Figures 11c to f) but also the potential for discrepancies. The discrepancies observed in AFs at the fundamental modes cover the range of possible accuracy achieved by the proposed approach. In cases where the best-estimate median site response does not capture the observed median well, the 5th and 95th percentiles of the median site response manage to better represent it, although with exceptions (e.g. SZOH37 around 10 Hz, SBSH08 around 2 Hz). Such high
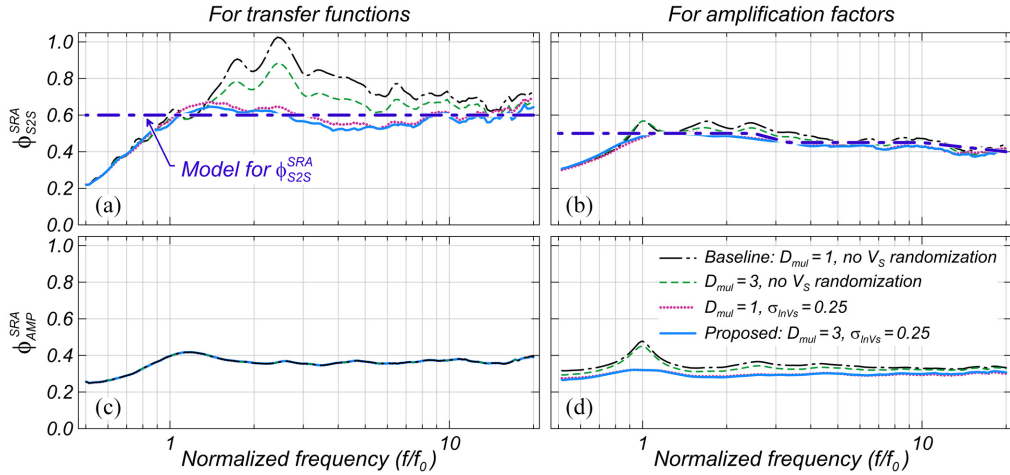
Figure 9. Comparison of site response residual standard deviations (ϕ_{S2S}^{SRA} and ϕ_{AMP}^{SRA}) in transfer functions (TFs) and amplification factors (AFs): (a) ϕ_{S2S}^{SRA} for TFs, (b) ϕ_{S2S}^{SRA} for AFs, (c) ϕ_{AMP}^{SRA} for TFs, and (d) ϕ_{AMP}^{SRA} for AFs.

amplitudes are explained by the additional variability in site response residuals, ϕ_{AMP}^{SRA}, whose effects are assumed to be included in the input motion in seismic hazard analyses, and thus not considered to address modeling errors in this study. Overall, the proposed approach provides more accurate site response predictions compared to a more traditional approach (i.e., baseline in Figure 11). A similar figure that shows the range of possible accuracy achieved by the proposed approach at high frequencies is presented in the Supplemental Appendix D.

Effect of sites' region and type

As previously described, c_{3D}^{SRA}, ϕ_{S2S}^{SRA}, and ϕ_{AMP}^{SRA} are quantified based on data from 495 3D-like borehole array sites from Japan and the United States (Figures 8 and 9). This approach is preferred as grouping the sites according to their compliance to the 1D assumptions (1D-like or 3D-like), or region as such an approach (1) requires a taxonomy for the identification of the site type when no ground-motion data are available, and (2) reduces the data to smaller groups of sites. In this section, c_{3D}^{SRA}, ϕ_{S2S}^{SRA}, and ϕ_{AMP}^{SRA} are calculated considering the sites' compliance to 1D assumptions and geographical location. While the geographical location is not expected to be a factor controlling site response, grouping the sites by their location either in Japan or California could capture geomorphological aspects and ground surface features (e.g., Nweke et al., 2022; Pilz et al., 2022) leading to differences in site response accuracy. There are 39 1D-like sites and 495 3D-like sites, 485 of them located in Japan, 9 in California, and 1 in Alaska. All 1D SRAs in this section are conducted considering $D_{mul} = 3$, and $\sigma_{\ln V_S} = 0.25$. A comparison of observed and theoretical TFs and AFs for the 39 1D-like sites is presented in Supplemental Appendices B and C of the companion paper, and TFs and AFs for the nine 3D-like sites in California in Supplemental Appendices A and B, respectively.

The site response residuals for 1D-like sites indicate underprediction at $f/f_0 = 1$ and overall lower standard deviations, compared to the 3D-like sites (Figure 12). c_{1D}^{SRA} (method
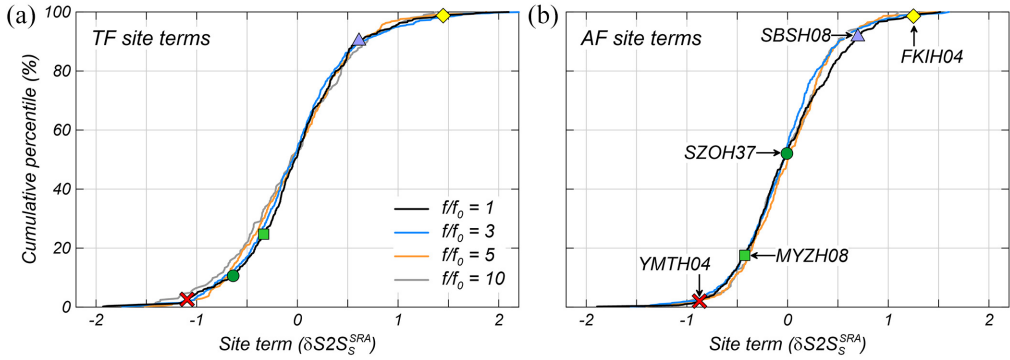
Figure 10. Cumulative distribution of site terms ($\delta S2S_s^{SRA}$) at $f/f_0 = 1, 3, 5,$ and 10: (a) $\delta S2S_s^{SRA}$ in transfer functions (TFs), and (b) $\delta S2S_s^{SRA}$ in amplification factors (AFs). Labels indicate five selected sites with approximately uniformly spaced site terms in AFs.

Table 3. Recommended models for method bias (c_{3D}^{SRA}) and standard deviations ϕ_{S2S}^{SRA} and ϕ_{AMP}^{SRA} of TFs and AFs for various normalized periods and frequencies

T/T_0	f/f_0	c_{3D}^{SRA}		ϕ_{S2S}^{SRA}	
		TF	AF	TF	AF
0.05	20.0	0.60	0.20	0.60	0.40
0.10	10.0	0.45	0.05	0.60	0.45
0.20	5.00	0.50	0.0	0.60	0.45
0.30	3.33	0.55	0.0	0.60	0.45
0.40	2.50	0.55	0.0	0.60	0.50
0.50	2.00	0.55	−0.05	0.60	0.50
0.60	1.67	0.55	−0.10	0.60	0.50
0.70	1.43	0.55	−0.15	0.60	0.50
0.80	1.25	0.40	−0.30	0.60	0.50
0.90	1.11	0.10	−0.50	0.60	0.50
0.95	1.05	−0.10	−0.55	0.60	0.50
1.00	1.00	−0.20	−0.63	0.60	0.50
1.05	0.95	−0.30	−0.63	0.60	0.50
1.10	0.91	−0.30	−0.63	0.60	0.50
1.20	0.83	−0.30	−0.63	0.60	0.50
1.30	0.77	−0.15	−0.55	0.60	0.50
1.40	0.71	−0.10	−0.45	0.60	0.50
1.50	0.67	−0.05	−0.40	0.60	0.50
1.60	0.63	0.0	−0.35	0.60	0.50
1.70	0.59	0.05	−0.33	0.60	0.50
1.80	0.56	0.05	−0.25	0.60	0.50
1.90	0.53	0.05	−0.25	0.60	0.50
2.00	0.50	0.05	−0.25	0.60	0.50

TF: transfer function; AF: amplification factor.

bias for 1D-like sites) shows an overall underprediction of the TFs in 0.5 ln units across frequencies (Figure 12a), whereas the AFs are nearly unbiased (Figure 12b). Compared to c_{3D}^{SRA}, c_{1D}^{SRA} tends toward an underprediction of the fundamental mode as opposed to the overprediction exhibited by c_{3D}^{SRA} (Figure 12 g and h). This tendency is expected as, unlike
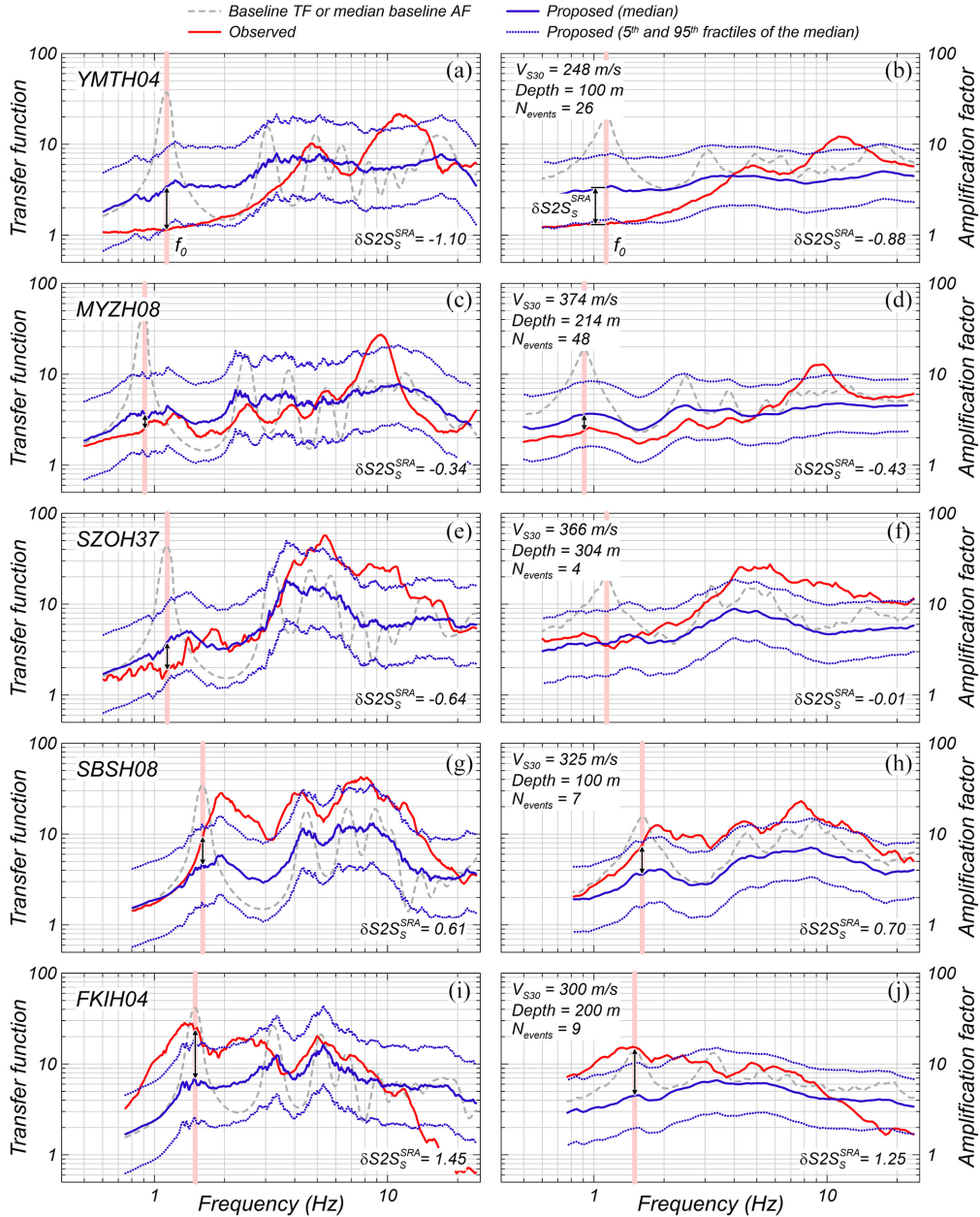
Figure 11. Transfer functions (TFs) and amplification factors (AFs) estimated using Cases 1 (baseline or theoretical) and Case 4 (proposed approach) for five KiK-net sites. The sites are selected to cover the range of site terms ($\delta S2S_s^{SRA}$) in AFs at the sites' fundamental frequency (f_0).

3D-like sites, the 1D-like sites often present a good agreement between the theoretical and observed TFs' fundamental modes. Therefore, the extent to which overpredictions occur at $f/f_0 = 1$ is reduced. ϕ_{S2S}^{SRA} for 1D-like sites (Figure 13a and b) is slightly higher or equal than ϕ_{S2S}^{SRA} for 3D-like sites at the fundamental mode, and mostly lower by 0.1–0.2 at higher frequencies. Finally, there is no significant difference in the estimated ϕ_{AMP}^{SRA}, except at f/f_0
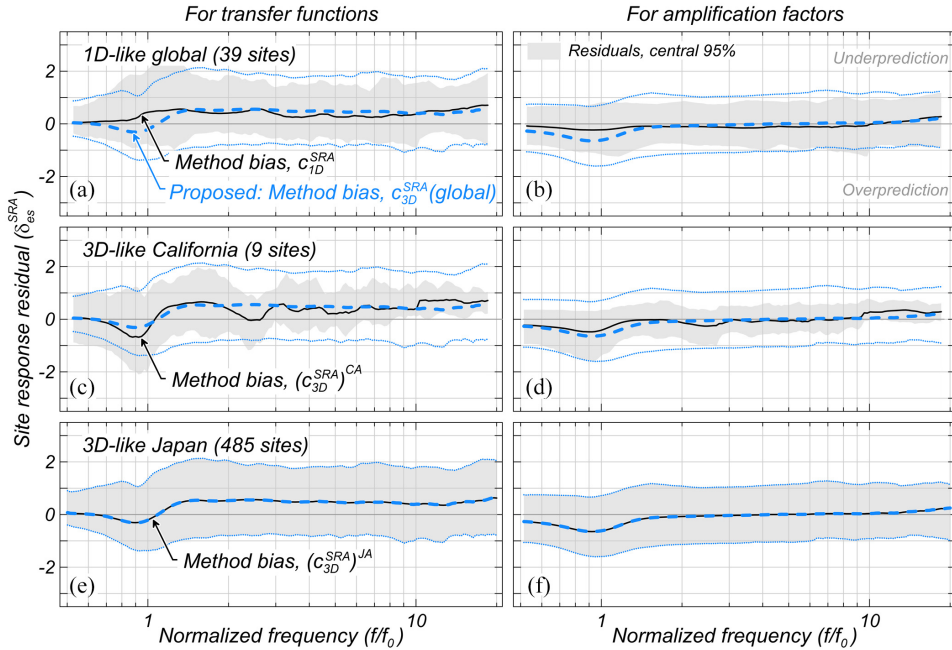
Figure 12. Comparison of site response method bias (c_{1D}^{SRA} or c_{3D}^{SRA}) and residuals (central 95%) in transfer functions and amplification factors estimated from different datasets: (a) and (b) 1D-like sites from Japan and the United States, (c) and (d) 3D-like sites from California, and (e) and (f) 3D-like sites from Japan.

higher than seven, where a slight reduction is observed for the 1D-like sites in both TFs and AFs.

The site response residuals for California are similar in the tendency to the global data, clearly dominated by the sites in Japan, but they show a different trend in the observed ϕ_{S2S}^{SRA} and ϕ_{AMP}^{SRA} across frequencies. c_{3D}^{SRA} for TFs for sites in California shows stronger under- and overpredictions, although with a similar trend with frequency (Figure 12c), whereas minor differences are observed in c_{3D}^{SRA} for AFs (Figure 12d). ϕ_{S2S}^{SRA} for TFs for sites in California is higher near the fundamental mode by about 0.3 (Figure 13a) and significantly lower at higher frequencies, with values nearing zero at some f/f_0. These near-zero values are given by the very limited data available for California that cannot capture a more realistic residual variability. ϕ_{S2S}^{SRA} for AFs for sites in California are consistently lower by about 0.2–0.3 ln units (Figure 13b) compared to ϕ_{S2S}^{SRA} based on the global dataset, and lower than ϕ_{S2S}^{SRA} estimated by Stewart and Afshari (2021) on average, although this difference could partly be attributed to the number of sites and recordings considered. There is no significant difference in the estimated ϕ_{AMP}^{SRA}, except an increase at f/f_0 lower than 1.1 and a consistent decrease at f/f_0 higher than eight. ϕ_{AMP}^{SRA} for California is consistent with findings by Stewart and Afshari (2021). The dataset from Japan represents 98% of the global dataset and thus results are nearly the same and not described. Unsurprisingly, these results indicate that the data from the United States do not contribute to the estimation of the recommended c_{3D}^{SRA}, ϕ_{S2S}^{SRA}, or ϕ_{AMP}^{SRA}.
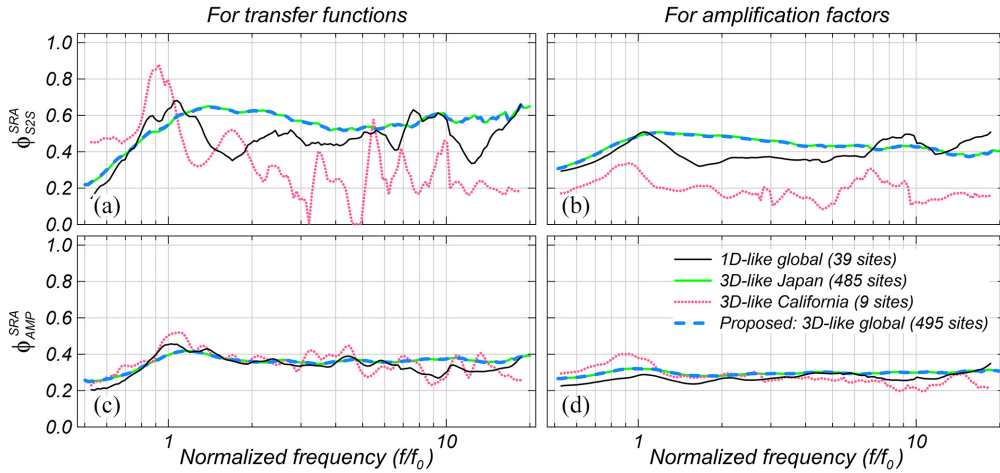
Figure 13. Comparison of site response residual standard deviations (ϕ_{S2S}^{SRA} and ϕ_{AMP}^{SRA}) in transfer functions (TFs) and amplification factors (AFs) estimated from different datasets: (1) 1D-like sites from Japan and the United States, (2) 3D-like sites from California, (3) 3D-like sites from Japan, and (4) 3D-like sites from Japan and the United States (proposed). (a) ϕ_{S2S}^{SRA} for TFs, (b) ϕ_{S2S}^{SRA} for AFs, (c) ϕ_{AMP}^{SRA} for TFs, and (d) ϕ_{AMP}^{SRA} for AFs.

Applicability to outcrop ground motions

The proposed approach is developed based on borehole array data, whereas forward site response predictions and ground-motion model developments are based on rock outcropping and free field data. Concerns regarding the use of borehole recordings are due to the wave-canceling effects that such recordings carry. The wave-canceling effect refers to the destructive interference of the upgoing and downgoing waves (Bonilla et al., 2002) that leads to near-zero amplitude at some frequencies in borehole recordings and thus unrealistically high amplitudes in observed TFs (e.g. site OKYH14 at 5 Hz in Figure 14e). Given that these TF amplitudes are not associated with the subsurface structure or site-specific factors controlling the site response, they are referred to as pseudo-resonances (Tao and Rathje, 2020b).

Various researchers investigated wave-canceling effects and proposed methods for using borehole array data (e.g. Cadet et al., 2011; Chandra et al., 2015; Clayton and Wiggins, 1976; Mehta et al., 2007; Parolai et al., 2010); however, no method is established to date. Tao and Rathje (2020a, 2020b) propose a taxonomy for identifying sites affected by pseudo-resonances and recommend that these sites not be used in site response validation studies. Contrary to this, Stewart and Afshari (2021) suggest that pseudo-resonances be embraced and considered in the evaluation of the 1D SRA predicting capabilities. While the effect of pseudo-resonances leads to the overestimation of TF amplitudes, in this study, the question we try to answer is whether pseudo-resonances affect the site response bias, c_{3D}^{SRA}, and the standard deviations of the site response residual components, ϕ_{S2S}^{SRA} and ϕ_{AMP}^{SRA}.

An initial investigation to evaluate the effect of pseudo-resonances on c_{3D}^{SRA}, ϕ_{S2S}^{SRA}, and ϕ_{AMP}^{SRA} is conducted with the aim to find any distinctive difference. To this end, sites not
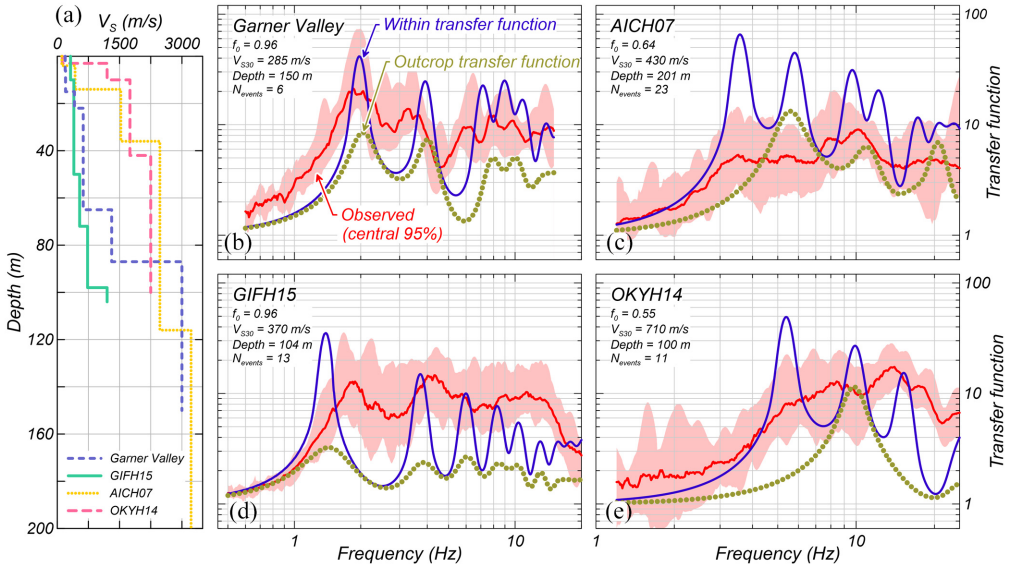
Figure 14. Example of sites unaffected and affected by pseudo-resonances: (a) measured V_S profiles, (b) and (d) transfer functions (TFs) for sites free of pseudo-resonances, (c) and (e) TFs for sites with pseudo-resonances.

affected by pseudo-resonances are first selected from the database. Tao and Rathje (2020b) suggest that true resonances are those captured by outcropping theoretical TFs (i.e. TFs calculated using the outcropping boundary condition), whereas pseudo-resonances are captured by within theoretical TFs. In addition, the authors indicate that the absence of a distinct velocity contrast in the V_S profile is suggestive of the presence of pseudo-resonances. Based on these observations, sites with similar f_0 from the outcropping and within TFs ($D_{mul} = 1$, no randomization) within 15% are considered free of pseudo-resonances. In cases where the similarity of the TFs alone does not suggest the presence or absence of pseudo-resonances, the site's V_S profile is inspected for velocity contrasts. Figure 14 shows examples of sites with and without pseudo-resonances, and a complete set of figures for all sites identified to be unaffected by pseudo-resonances is presented in Supplemental Appendix C. Any discrepancies between the theoretical and observed TFs is not considered in this selection and rather attributed to 3D effects.

The 495 sites used for the statistical analysis are separated into 40 sites identified as free of pseudo-resonances (N-P), and the remaining 455 sites with pseudo-resonances (P). Residuals are computed for each group, and the statistical analyses conducted to recompute c_{3D}^{SRA}, ϕ_{S2S}^{SRA}, and ϕ_{AMP}^{SRA}. The results show minor differences between $(c_{3D}^{SRA})^P$, $(\phi_{S2S}^{SRA})^P$, and $(\phi_{AMP}^{SRA})^P$ (Figures 15c to d and 16) and the proposed global c_{3D}^{SRA}, ϕ_{S2S}^{SRA}, and ϕ_{AMP}^{SRA} (Figures 8 g to h and 9). The method bias $(c_{3D}^{SRA})^{N-P}$ is higher than $(c_{3D}^{SRA})^P$ by 0.3–0.7 for TFs and 0.5 for AFs at f/f_0 lower than 2, whereas it is slightly lower at higher frequencies (Figure 15). The standard deviation $(\phi_{S2S}^{SRA})^{N-P}$ is higher than $(\phi_{S2S}^{SRA})^P$ by about 0.2 and 0.15 for TFs and AFs around the fundamental mode, and by about 0.3 and 0.2 for TFs and AFs starting at $f/f_0 = 10$ (Figure 15c and d). Finally, the standard deviations $(\phi_{AMP}^{SRA})^{N-P}$ and $(\phi_{S2S}^{SRA})^P$ fluctuate within a 0.05 range (Figure 16e and f).

Overall, results for sites considered unaffected by pseudo-resonances indicate higher c_{3D}^{SRA} for f/f_0 up to around 3 and higher ϕ_{S2S}^{SRA} around $f/f_0 = 1$ and higher than 9. To
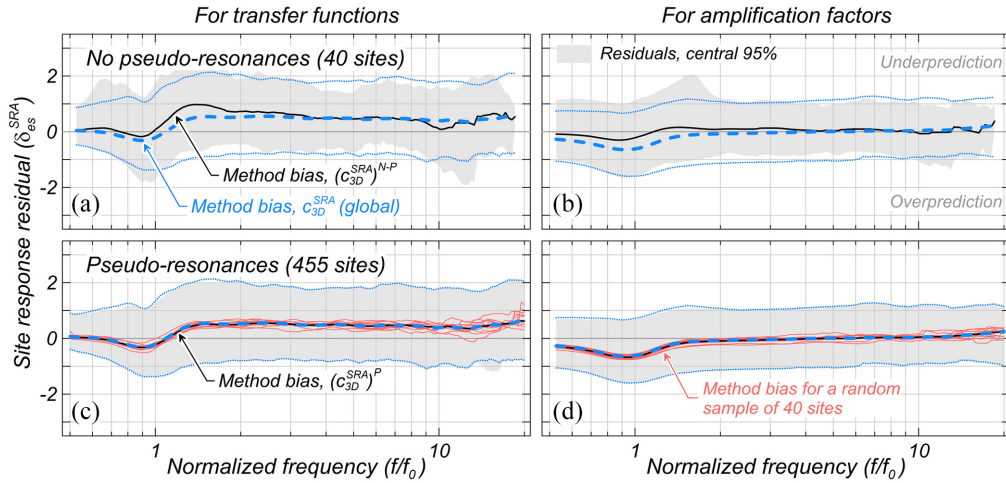
Figure 15. Comparison of site response method bias (c_{3D}^{SRA}) and residuals (central 95%) in transfer functions and amplification factors estimated from different datasets. (a) and (b) sites unaffected by pseudo-resonances, (c) and (d) sites affected by pseudo-resonances.
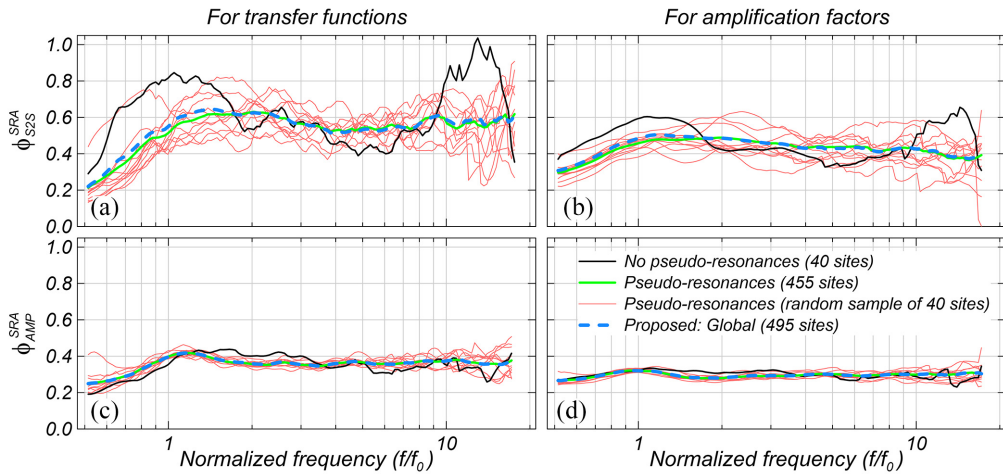

Figure 16. Comparison of site response residual standard deviations (ϕ_{S2S}^{SRA} and ϕ_{AMP}^{SRA}) in transfer functions (TFs) and amplification factors (AFs) estimated from different datasets: (1) sites unaffected by pseudo-resonances, (2) sites affected by pseudo-resonances, (3) random sample of sites affected by pseudo-resonances, and (4) sites unaffected and affected by pseudo-resonances (proposed). (a) ϕ_{S2S}^{SRA} for TFs, (b) ϕ_{S2S}^{SRA} for AFs, (c) ϕ_{AMP}^{SRA} for TFs, and (d) ϕ_{AMP}^{SRA} for AFs.

remove the effect of the lower number of sites free of pseudo-resonances, mixed-effects regressions are conducted for suites of 40 sites randomly sampled without replacement from the dataset of 455 sites affected by pseudo-resonances. The results confirmed the observed trends (Figure 16) and variability at intermediate frequencies. Similar to the results for 1D-like sites, the higher c_{3D}^{SRA} and ϕ_{S2S}^{SRA} values near f_0 are due to the similarity in the theoretical and observed TFs' fundamental modes.
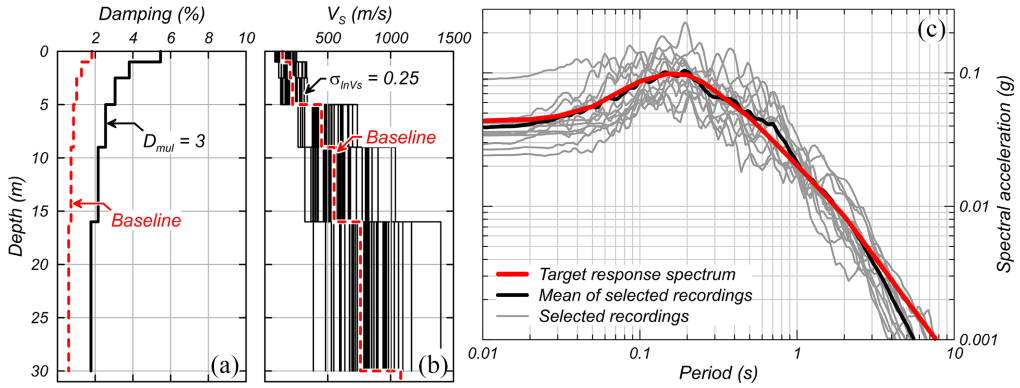
Figure 17. (a) Baseline and factorized damping profiles. (b) Baseline and randomized V_S profiles. (c) Target response spectrum and selected input ground motions.

These findings show that there is potential for further underprediction of the median site response, and higher ϕ_{S2S}^{SRA} and ϕ_{AMP}^{SRA} in applications using outcropping ground-motion recordings. Given (1) the relatively low number of sites free of pseudo-resonances, (2) the assumptions made in the selection of such sites, and (3) the impact that these results would have on site response and seismic hazard studies, the values for c_{3D}^{SRA} and ϕ_{S2S}^{SRA} in Table 3 are still preferred for practical applications. The results presented in this section encourage the need for further investigations regarding the applicability of borehole array data-based lessons to outcropping applications.

Example application

The proposed approach is used to estimate the site response at a hypothetical project site selected for the construction of a rigid structure with a period of approximately 0.1 s. The site is located on 30-m-thick old deposit of dense alluvial soils overlying a bedrock with $V_S = 1080$ m/s at the top 30 m. A single measured V_S profile available for the site (Figure 17b). The closest active fault is located 25 km away from the site, and the highest historical earthquake magnitude is $M_w6.0$. The engineers leading the design of the structure are concerned about the seismic demands during an earthquake of similar magnitude and with a predominant period close to the structure's resonant period. The analysts decide to conduct a deterministic seismic hazard analysis and 1D SRAs to estimate the seismic demand at the foundation level of the structure, assuming free field conditions.

Seismic demand

A deterministic scenario is defined based on the site's characteristics, and the response spectrum estimated using the Abrahamson et al. (2014) GMM (Figure 17c). For practical purposes, this spectrum is considered representative of the seismic demand at the base of the alluvial deposit. A more appropriate estimation requires (1) accounting for the differences in the site-specific V_S profiles and the implied by the GMM (Williams and Abrahamson, 2021), (2) the application of the input ground motions at the bottom of the deposit, and (3) the estimation of the response spectrum at surface using a single-station sigma given that the site response is estimated using 1D SRAs (e.g. Al Atik, 2015).

Thirteen ground motions are selected from the NGA-West2 database (Ancheta et al., 2013) and scaled such that their mean approximately matches the target response spectrum (Figure 17c). The potential for soil nonlinearity is evaluated based on the shear strain index, I_γ, with V_{S30} = 450 m/s. All I_γ values are lower than 0.005%, thus linear elastic SRAs are appropriate, and the proposed approach is well suited for estimating the site response.

Proposed approach

Step 1: site characterization. The site characterization consists of estimating the baseline V_S profile, and laboratory-based damping profile. The baseline V_S profile is taken from the available field measurement (Figure 17b), whereas the damping profile is estimated after Darendeli (2001), considering the mean effective stress at the middle of each V_S layer (Figure 17a). The site's f_0 values based on its within and outcropping TFs are 5.65 and 7.93 Hz, respectively.

Step 2: site response input parameters. The baseline damping and V_S profiles are adjusted to remove the errors intrinsic to 1D SRAs as a tool and improve the accuracy of site response predictions. The small-strain damping profile estimated after Darendeli (2001) is increased by D_{mul} = 3. In addition, the top 30 m of the baseline V_S profile corresponding to the alluvial deposit are randomized to generate 50 V_S profiles using the V_S model after Toro (1995) with $\sigma_{\ln V_S} = 0.25$. The other parameters used for the Toro model are those recommended by Toro for sites with V_{S30} from 180 to 360 m/s. The obtained damping and randomized V_S profiles are shown in Figure 17.

Step 3: uncorrected median site response. The input ground motions are propagated through each of the randomized V_S profiles to obtain the response at ground surface (Figure 18). An outcropping boundary condition is considered for the base of the models. Fifty FAS and acceleration response spectra per input ground motion are obtained at surface, and the median values considered the uncorrected (biased) best-estimate responses for each one of the input motions (Figure 18e and f). Results are presented in FAS from 0.04 to 0.25 s (half $f_0 \approx 4$ Hz, to 25 Hz), but PSA at shorter periods are also presented as they are often controlled by the longer period range (Douglas and Boore, 2011). FAS and PSA estimates at periods longer the site's fundamental mode can be estimated using GMM (e.g. Bayless and Abrahamson, 2019).

Step 4: bias correction. The median FAS and PSA response spectrum at ground surface are corrected to account for the 1D-SRA bias. The bias correction is conducted by scaling T/T_0 in Table 3 by the site's fundamental period ($T_0 \approx 0.125$ s) and then adding the c_{3D}^{SRA} values for TFs or AFs to the natural logarithm of the median responses obtained in Step 3. The resulting bias-corrected FAS and PSA are the best-estimate median site response for a given input motion. These results are presented in arithmetic units in Figure 18g and h for TFs and AFs, respectively.

Step 5: accounting for modeling errors. The bias-corrected best-estimate TFs and AFs assume that the proposed approach and 1D SRAs are capable of perfectly estimating the site response, which is unrealistic. To account for the potential response to be higher or lower due to unmodeled features affecting the response with a 90% confidence interval, the best-estimate bias-corrected median TF and AF are shifted by $\pm 1.65 \times \phi_{S2S}^{SRA}$. The resulting 5th
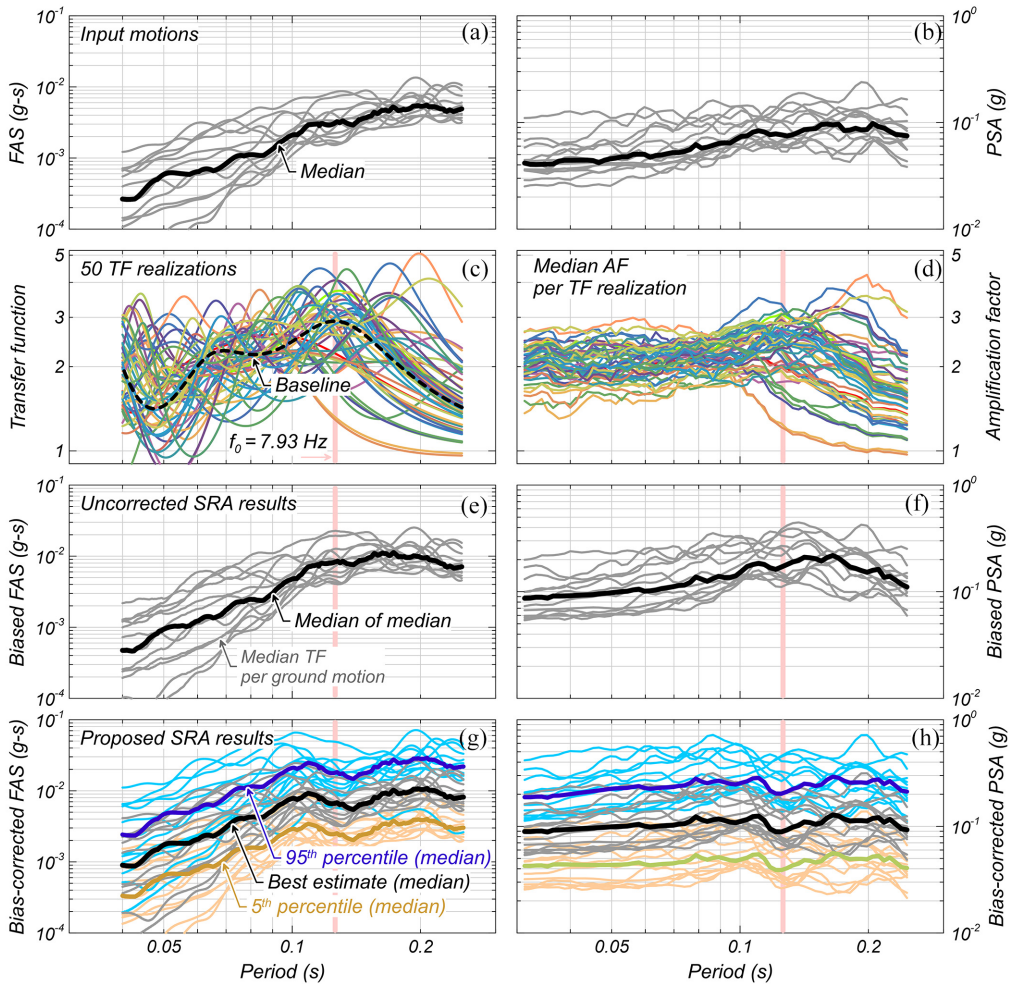
Figure 18. Estimated site response for a hypothetical site, step-by-step results for Fourier amplitude spectra (FAS) and pseudo-spectral acceleration (PSA) response spectra: (a) and (b) input ground motions, (c) and (d) transfer functions and amplification factors (median of all input motions) per randomized V_S profile; (e) and (f) uncorrected FAS and uncorrected PSA response spectra (median of all input motions) at surface; (g) and (h) best-estimate, and 5th and 95th percentiles of bias-corrected FAS and PSA response spectrum at surface (median of all input motions).

and 95th percentiles of the median site response for each one of the input ground motions are presented in Figures 18g and h.

Recommended path forward

The site response evaluation indicates that the median PSA expected at a period of 0.1 s is approximately 0.145g. However, when accounting for modeling errors, it is possible that the PSA be 0.32g (median with 90% confidence interval). Whether the best-estimate median PSA or 95th percentile of the median PSA is used for design of the structure depends on the project-specific engineering- and non-engineering-related aspects. However, it is

recommended that (1) the bias-corrected best-estimate median site response be used for design and (2) the 95th median site response percentile be checked. Using the 95th percentile median site response allows the responsible team to adjust the design to prevent a potential catastrophic failure, or to make an informed decision about the best path forward.

Conclusions

An approach for conducting linear elastic 1D SRAs developed based on borehole array data was presented. This approach (1) uses a damping multiplier ($D_{\mathrm{mul}} = 3$) and V_S randomization ($\sigma_{\ln V_S} = 0.25$) to improve site response predictions and (2) accounts for the 1D-SRA bias ($c_{\mathrm{3D}}^{\mathrm{SRA}}$) and the modeling errors, quantified through the standard deviation $\phi_{\mathrm{S2S}}^{\mathrm{SRA}}$, due to the inability of 1D SRAs to capture non-1D effects affecting site response. Current engineering practice expects 1D SRAs to provide accurate site response estimates and neglects modeling errors. This is an unrealistic expectation.

Comparisons of ground-motion data from 534 borehole array sites against 1D SRA predictions in terms of transfer functions (TFs) and amplification factors (AFs) showed global trends in the discrepancies. An overall site response overprediction is observed in the low-frequency range and underpredictions in the high-frequency range. The use of randomized V_S profiles reduces the overpredictions at the frequency modes and leads to median TFs and AFs with a more uniform distribution of energy (i.e. site response amplitudes) across frequencies, similar to empirical median responses. The use of $D_{\mathrm{mul}} = 3$ to increase damping leads to the estimation of nearly unbiased AFs across frequencies. Despite these improvements, site response estimates from 1D SRAs conducted with D_{mul} and randomized V_S profiles are still biased and present significant variability in their site terms ($\delta S2S_{\mathrm{s}}^{\mathrm{SRA}}$). The proposed approach addresses these concerns by bias-correcting the predicted responses and considering the 5th and 95th percentiles of the median site response.

An investigation of the effect of pseudo-resonances on the proposed approach indicates that outcropping applications could potentially require a stronger bias-correction to prevent underpredictions and a larger shift of the bias-corrected median response to account for 1D SRA modeling errors. This finding further stresses the need for investigating the applicability of findings from site response studies using borehole array data for engineering applications. Given the assumptions made in this investigation and recognizing that current practices assume $c_{\mathrm{3D}}^{\mathrm{SRA}} = 0$ and $\phi_{\mathrm{S2S}}^{\mathrm{SRA}} = 0$, using the proposed estimates is considered a step forward in engineering practice regardless of the potential issues associated with borehole array data.

The recommended values for $c_{\mathrm{3D}}^{\mathrm{SRA}}$ and $\phi_{\mathrm{S2S}}^{\mathrm{SRA}}$ are fundamentally associated to the procedures followed in the development of the proposed approach for conducting 1D SRAs. Thus, all five steps provided under section "Proposed approach" should be followed. Reducing the magnitude of the recommended $\phi_{\mathrm{S2S}}^{\mathrm{SRA}}$ would likely require conducting 2D or 3D SRAs and considering the $\phi_{\mathrm{S2S}}^{\mathrm{SRA}}$ associated with those numerical approaches. The proposed $c_{\mathrm{3D}}^{\mathrm{SRA}}$ and $\phi_{\mathrm{S2S}}^{\mathrm{SRA}}$ are valid for linear elastic analyses only, but the presented framework for comparing borehole array data against 1D SRA-based predictions using randomized V_S profiles could be followed to develop $c_{\mathrm{3D}}^{\mathrm{SRA}}$ and $\phi_{\mathrm{S2S}}^{\mathrm{SRA}}$ models applicable to nonlinear SRAs.

Declaration of conflicting interests

Funding

ORCID iDs

Renmin Pretell https://orcid.org/0000-0001-8552-2905
Katerina Ziotopoulou https://orcid.org/0000-0001-5494-497X

Supplemental material

Supplemental material for this article is available online.

References

Abrahamson NA, Silva WJ and Kamai R (2014) Summary of Abrahamson and Silva NGA ground-motion relation for active crustal regions. *Earthquake Spectra* 30(3): 1025–1055.

Abrahamson NA, Somerville PG and Cornell CA (1990) Uncertainty in numerical strong motion predictions. In: *Proceedings of the 4th US national conference on earthquake engineering*, vol. 1, Palm Springs, CA, 20–24 May, pp. 407–416. El Cerrito, CA: Earthquake Engineering Research Institute.

Afshari K, Stewart JP and Steidl JH (2019) California ground motion vertical array database. *Earthquake Spectra* 35(4): 2003–2015.

Al Atik (2015) NGA-East: Ground-motion *standard deviation models for central* and Eastern North America. Report PEER 2015/07, 1 June. Berkeley, CA: Pacific Earthquake Engineering Research Center, University of California, Berkeley.

Al Atik L, Abrahamson N, Bommer JJ, Scherbaum F, Cotton F and Kuehn N (2010) The variability of ground-motion prediction models and its components. *Seismological Research Letters* 81: 794–801.

Ancheta TD, Darragh RB, Stewart JP, Seyhan E, Silva WJ, Chiou BSJ, Wooddell KE, Graves RW, Kottke AR, Boore DM, Kishida T and Donahue JL (2013) PEER N*GA-W*est2 *d*atabase. Report PEER 2013/03, 2 May. Berkeley, CA: Pacific Earthquake Engineering Research Center, University of California, Berkeley.

Aoi S, Kunugi T and Fujiwara H (2004) Strong-motion seismograph network operated by NIED: K-NET and KiK-net. *Journal of Japan Association for Earthquake Engineering* 4(3): 65–74.

Atkinson GM (2006) Single-station sigma. *Bulletin of the Seismological Society of America* 96(2): 446–455.

Bayless J and Abrahamson NA (2019) Summary of the BA18 ground-motion model for Fourier amplitude spectra for crustal earthquakes in California. *Bulletin of the Seismological Society of America* 109(5): 2088–2105.

Bazzurro P and Cornell CA (2004) Nonlinear soil site effects in probabilistic seismic hazard analysis. *Bulletin of the Seismological Society of America* 94: 2110–2123.

Bonilla LF, Steidl JH, Gariel J-C and Archuleta RJ (2002) Borehole response studies at the Garner Valley Downhole Array, Southern California. *Bulletin of the Seismological Society of America* 92(8): 3165–3179.

Boore DM (2003) Prediction of ground motion using the stochastic method. *Pure and Applied Geophysics* 160: 635–676.

Boore DM (2005) *SMSIM–Fortran programs for simulating ground motions from earthquakes: Version 2.3–a revision of OFR 96–80-A*. Open file report 00–509, 15 August. Menlo Park, CA: U.S. Geological Survey.

Cadet H, Bard P-Y and Rodriguez-Marek A (2011) Site effect assessment using KiK-net data: Part 1. A simple correction procedure for surface/downhole spectral ratios. *Bulletin of Earthquake Engineering* 10(2): 421–448.

Chandra J, Gueguen P, Steidl JH and Bonilla LF (2015) In situ assessment of the G-γ curve for characterizing the nonlinear response of soil: Application to the Garner Valley Downhole Array and the Wildlife Liquefaction Array. *Bulletin of the Seismological Society of America* 105(2A): 993–1010.

Clayton RW and Wiggins RA (1976) Source shape estimation and deconvolution of teleseismic body waves. *Journal of the Royal Astronomical Society* 47: 151–177.

Darendeli MB (2001) *Development of a new family of normalized modulus reduction and material damping curves*. PhD Dissertation, The University of Texas at Austin, Austin, TX.

de la Torre CA, Bradley BA and McGann CR (2021) 2D geotechnical site-response analysis including soil heterogeneity and wave scattering. *Earthquake Spectra* 38(2): 1124–1147.

Douglas J and Boore DM (2011) High-frequency filtering of strong motion records. *Bulletin of Earthquake Engineering* 9: 395–409.

Electric Power Research Institute (EPRI) (2013) *Seismic evaluation guidance: Screening, prioritization and implementation details (SPID) for the resolution of Fukushima near term task force recommendation 2.1. Seismic*. Report 1025287, 28 February. Palo Alto, CA: EPRI.

Gibbs JF, Tinsley JC, Boore DM and Joyner WB (2000) *Borehole velocity measurements and geological conditions at thirteen sites in the Los Angeles, California region*. Open File Report 00–470, 1 June. Menlo Park, CA: U.S. Geological Survey.

Hashash YMA, Musgrove MI, Harmon JA, Ilhan O, Xing G, Numanoglu O, Groholski DR, Phillips CA and Park D (2020) *DEEPSOIL 7, User Manual*. Urbana, IL: Board of Trustees of University of Illinois at Urbana-Champaign.

Haskell NA (1953) The dispersion of surface waves on multilayered media. *Bulletin of the Seismological Society of America* 72: 17–34.

Holzer TL and Youd TL (2007) Liquefaction, ground oscillation, and soil deformation at the Wildlife Array, California. *Bulletin of the Seismological Society of America* 97(3): 961–976.

Idriss IM (2011) Use of V_{S30} to represent local site conditions. In: *Fourth international association of seismology and physics of the earth's interior/international association of earthquake engineering international symposium on the effects of surface geology on seismic motion(ESG4)*, Santa Barbara, CA, 23–26 August.

Jones JM, Kalkan E, Stephens CD and Peter Ng (2017) *PRISM Software–Processing and Review Interface for Strong-Motion Data: U.S. Geological Survey Techniques and Methods* (Book 12, Chapter A2). Reston, VA: U.S. Geological Survey.

Joyner WB, Warrick RE and Fumal TE (1981) The effect of quaternary alluvium on strong ground motion in the Coyote Lake, California, earthquake of 1979. *Bulletin of the Seismological Society of America* 71: 1333–1349.

Kaklamanos J and Bradley BA (2018) Challenges in Predicting Seismic Site Response with 1D Analyses: Conclusions from 114 KiK-net Vertical Seismometer Arrays. *Bulletin of the Seismological Society of America* 108(5): 2816–2838.

Kaklamanos J, Bradley BA, Moolacattu AN and Picard BM (2020) Physical hypotheses for adjusting coarse profiles and improving 1D site response estimation assessed at 10 KiK-net sites. *Bulletin of the Seismological Society of America* 110(3): 1338–1358.

Kaklamanos J, Bradley BA, Thompson EM and Baise LG (2013) Critical parameters affecting bias and variability in site-response analyses using KiK-net downhole array data. *Bulletin of the Seismological Society of America* 103: 1733–1749.

Kalkan E (2016) An automatic P-phase arrival time picker. *Bulletin of the Seismological Society of America* 106(3): 971–986.

Kalkan E (2021) *Frequency-Domain Zero-Padding Resampling (Interpolation)*. MATLAB Central File Exchange. Available at: www.mathworks.com/matlabcentral/fileexchange/58854-frequency-domain-zero-padding-resampling-interpolation (accessed 12 December, 2021).

Katsumata A (1996) Comparison of magnitudes estimated by the Japan meteorological agency with moment magnitudes for intermediate and deep earthquakes. *Bulletin of the Seismological Society of America* 86(3): 832–842.

Kim B, Hashash YMA, Stewart JP, Rathje EM, Harmon JA, Musgrove MI, Campbell KW and Silva WJ (2016) Relative differences between nonlinear and equivalent-linear 1-D site response analyses. *Earthquake Spectra* 32(3): 1845–1865.

Konno K and Ohmachi T (1998) Ground-motion characteristics estimated from spectral ratio between horizontal and vertical components of microtremor. *Bulletin of the Seismological Society of America* 88(1): 228–241.

Kottke AR (2018) *pyRotD v0.5.4*. Zenodo. DOI: 10.5281/zenodo.1322849.

Kottke AR and Rathje EM (2008) *Technical manual for Strata*. Report No: 2008/10, December. Berkeley, CA: Pacific Earthquake Engineering Research Center, University of California, Berkeley.

Kwok AOL, Stewart JP, Hashash YMA, Matasovic N, Pyke R, Wang Z and Yang Z (2007) Use of exact solutions of wave propagation problems to guide implementation of nonlinear seismic ground response analysis procedures. *Journal of Geotechnical and Geoenvironmental Engineering* 133(11): 1385–1398.

Lyons RG (2014) *Understanding Digital Signal Processing*. 3rd ed. Hoboken, NJ: Prentice Hall.

Massa M, Pacor F, Luzi L, Bindi D, Milana G, Sabetta F, Gorini A and Marcucci S (2010) The ITalian ACcelerometric Archive (ITACA)—processing of strong-motion data. *Bulletin of Earthquake Engineering* 8(5): 1175–1187.

Mehta K, Snieder R and Graizer V (2007) Downhole receiver function: A case study. *Bulletin of the Seismological Society of America* 97(5): 1396–1403.

Menq FY (2003) *Dynamic properties of sandy and gravelly soils*. PhD Dissertation, The University of Texas at Austin, Austin, TX.

Nakamura Y (2019) What is the Nakamura method? *Seismological Research Letters* 90: 1437–1443.

National Research Institute for Earth Science and Disaster Resilience (NIED) (2019) *NIED K-NET, KiK-Net*. Tsukuba, Japan: NIED. DOI: 10.17598/NIED.0004.

Nweke CC, Stewart JP, Wang P and Brandenberg SJ (2022) Site response of sedimentary basin and other geomorphic provinces in southern California. *Earthquake Spectra* 38(4): 2341–2370.

Ordonez G (2012) *SHAKE2000—A Computer Program for the 1D Analysis of Geotechnical Earthquake Engineering Problems*. Washington, DC: GeoMotions, LLC.

Parolai S, Bindi D, Ansal A, Kurtulus A, Strollo A and Zschau J (2010) Determination of shallow S-wave attenuation by down-hole waveform deconvolution: A case study in Istanbul (Turkey). *Geophysical Journal International* 181: 1147–1158.

Passeri F (2019) *Development of an advanced geostatistical model for shear wave velocity profiles to manage uncertainties and variabilities in ground response analyses*. PhD Dissertation, Politecnico di Torino, Torino.

Passeri F, Foti S, Cox BR and Rodriguez-Marek A (2019) Influence of epistemic uncertainty in shear wave velocity on seismic ground response analyses. *Earthquake Spectra* 35(2): 929–954.

Pehlivan M, Rathje EM and Gilbert RB (2016) Factors influencing soil surface hazard curves. *Soil Dynamics and Earthquake Engineering* 83(2016): 180–190.

Pilz M, Cotton F and Zhu C (2022) How much are sites affected by 2-D and 3-D site effects? A study based on single-station earthquake records and implications for ground motion modeling. *Geophysics Journal International* 228: 1992–2004.

Pinheiro J, Bates D, DebRoy S and Sarkar D (2022) *NLME: Linear and Nonlinear Mixed Effects Models*. Vienna: R Foundation for Statistical Computing.

Pretell R, Abrahamson NA and Ziotopoulou K (2023) A borehole array data-based approach for conducting 1D site response analyses I: Damping and V_S randomization. *Earthquake Spectra*. DOI: 10.1177/87552930231173445

Pretell R, Ziotopoulou K and Abrahamson NA (2022) Conducting 1D site response analyses to capture 2D V_S spatial variability effects. *Earthquake Spectra* 38(3): 2235–2259.

Rodriguez-Marek A, Bommer JJ, Youngs RR, Crespo MJ, Stafford PJ and Bahrampouri M (2020) Capturing epistemic uncertainty in site response. *Earthquake Spectra* 37(2): 921–936.

Rodriguez-Marek A, Cotton F, Abrahamson NA, Akkar S, Al Atik L, Edwards B, Montalva GA and Dawood HM (2013) A model for single-station standard deviation using data from various tectonic regions. *Bulletin of the Seismological Society of America* 103: 3149–3163.

Rodriguez-Marek A, Montalva GA, Cotton F and Bonilla F (2011) Analysis of single-station standard deviation using the KiK-net data. *Bulletin of the Seismological Society of America* 101: 1242–1258.

Rodriguez-Marek A, Rathje E, Ake J, Munson C, Stovall S, Weaver T, Ulmer K and Juckett M (2021) *Documentation Report for SSHAC Level 2: Site Response* (RIL2021-15, November). San Antonio, TX: Research Information Letter, Office of Nuclear Regulatory Research.

Rodriguez-Marek A, Rathje E, Bommer J, Scherbaum F and Stafford P (2014) Application of single-station sigma and site-response characterization in a probabilistic seismic-hazard analysis for a new nuclear site. *Bulletin of the Seismological Society of America* 104(4): 1601–1619.

Stewart JP, Afshari KA and Hashash YMA (2014) *Guidelines for performing hazard-consistent one-dimensional ground response analysis for ground motion prediction.* Report no. 2014/16, October. Berkeley, CA: Pacific Earthquake Engineering Research Center, University of California, Berkeley.

Stewart JP and Afshari K (2021) Epistemic uncertainty in site response as derived from one-dimensional ground response analysis. *Journal of Geotechnical and Geoenvironmental Engineering* 147(1): 04020146.

Tao Y and Rathje E (2020a) Taxonomy for evaluating the site-specific applicability of one-dimensional ground response analysis. *Soil Dynamics and Earthquake Engineering* 128(2020): 105865.

Tao Y and Rathje E (2020b) The importance of distinguishing pseudoresonances and outcrop resonances in downhole array data. *Bulletin of the Seismological Society of America* 110(1): 288–294.

Thompson EM, Baise LG, Kayen RE and Guzina BB (2009) Impediments to predicting site response: Seismic property estimation and modeling simplifications. *Bulletin of the Seismological Society of America* 99(5): 2927–2949.

Thompson EM, Baise LG, Tanaka Y and Kayen RE (2012) A taxonomy of site response complexity. *Soil Dynamics and Earthquake Engineering* 41: 32–43.

Thompson EM, Kayen RE, Carkin B and Tanaka H (2010) *Surface-wave site characterization at 52 strong-motion recording stations affected by the Parkfield, California, M6.0 Earthquake of 28 September 2004.* Open File report 2010–1168. Reston, VA: U.S. Geological Survey.

Thomson WT (1950) Transmission of elastic waves through a stratified solid. *Journal of Applied Physics* 21: 89–93.

Thornley J, Dutta U, Fahringer P and Yang Z(J) (2019) In situ shear-wave velocity measurements at the Delaney Park downhole array, Anchorage, Alaska. *Seismological Research Letters* 90(1): 395–400.

Toro GR (1995) *Probabilistic models of the site velocity profiles for generic and site-specific ground-motion amplification studies.* Report 779574, 17 November. Upton, NY: Brookhaven National Laboratory.

Williams T and Abrahamson N (2021) Site-response analysis using the shear wave velocity profile correction approach. *Bulletin of the Seismological Society of America* 111(4): 1989–2004.

Zhu C, Cotton F, Kawase H, Haendel A, Pilz M and Nakano K (2022) How well can we predict earthquake site response so far? Site-specific approaches. *Earthquake Spectra* 38(2): 1047–1075.